CALGRID: A Mesoscale Photochemical Grid Model

Model Formulation Document

June 1989

by

R.J. Yamartino
J.S. Scire
S.R. Hanna
Sigma Research Corporation

and

G.R. Carmichael
Y.S. Chang
Chemical Engineering Department
University of Iowa

Report No. A049-1

Prepared for

California Air Resources Board
1131 S Street
Sacramento, California 95814

LIBRARY-AIR RESOURCES BOARD

Table of Contents

	Page
1. Introduction and Objectives	1
2. Model Structure and Computer Code Design	4
2.1 Design Objectives	4
2.2 Program Control and Options	6
2.3 Operator Splitting	7
3. Numerical Methods for Pollutant Transport	9
3.1 Horizontal Advection and Diffusion	9
3.1.1 Chapeau Function fromulation on an Arbitrary Grid	11
3.1.2 Advection Fidelity and Filtering	14
3.1.3 Advection Scheme Performance and Numerical Diffusion	17
3.1.4 Explicit Horizontal Diffusion	30
3.2 Vertical Level Scheme and Transport	30
3.2.1 Vertical Level Scheme and Associated Compensations	30
3.2.2 Vertical Transport	34
4. Horizontal and Vertical Diffusivity	38
4.1 Horizontal Diffusion	38
4.2 Vertical Diffusion	39
5. Dry Deposition	47
5.1 Deposition of Gases	53
5.2 Deposition of Particulate Matter	60
6. Integration of the Chemical Kinetics Equations	63
6.1 Introduction	63
6.2 Numerical Integration of the Chemistry Equations	63
6.3 Inclusion of Chemical Mechanism into the Calgrid Model	72
6.4 Sample Results Using the Updated Chemical Integration Formulation	78
References	82

Section 1

Introduction and Objectives

In July 1987 the California Air Resources Board initiated a project to upgrade and modernize the Urban Airshed Model (UAM). It was specified that the new model contain state-of-the-science improvements including:

- A vertical transport and diffusion scheme that incorporates the latest boundary layer formulations, permits arbitrary spacing of vertical levels, and accounts for all vertical flux components with moving or stationary levels.

- A full resistance-based model for the computation of dry deposition rates as a function of geophysical parameters, meteorological conditions, and pollutant species.

- A chemical integration solver based on the quasi-steady state method of Hesstvedt et al. (1978) and Lamb (1984). Such a solver can efficiently and accurately handle the stiffest of modern schemes.

- A more modern photochemical scheme such as the Carter, Atkinson, Lurmann, Lloyd (CALL) scheme developed for the ARB under a separate contract to the State Air Pollution Research Center. This family of schemes is now referred to as the SAPRC mechanisms.

- A horizontal advection scheme based on cubic splines or Chapeau functions that conserves mass exactly, prohibits negative concentrations, and exhibits very little numerical diffusion.

- New, structured ANSI 77 Fortran computer code that is highly modular, machine independent, and designed to facilitate a high degree of vectorization. The code also includes extensive internal documentation and contains the flexibility of dynamic memory allocation to facilitate efficient computer usage over a wide range of potential applications.

Our first task was to dissect the existing UAM to determine those portions that needed to be replaced. When the UAM was developed over a decade ago, computers and computer languages were very different than they are today. Computers, for example, tended to have small amounts of core storage memory. As a result of this, UAM developers adopted innovative methods to save memory, such as having the option to split up the grid, which created the need for additional intermediate data files and input/output (I/O) overhead. In addition the FORTRAN language had not yet experienced the beneficial impacts of structured programming concepts. The UAM code also clearly reflected years of modification and correction by a number of programmers and scientists. Thus, after several months of effort we made the difficult decision to start over "from scratch" and build a new model. As we were simultaneously constructing a new non-steady-state dispersion model (CALPUFF) and associated meteorological driver package (CALMET), it was decided that the new photochemical model should be driven by (or drivable by) CALMET. Thus, it has been given the new name CALGRID, both to indicate that it is no longer "just" an updated UAM, but also to suggest that it can be run "in parallel" with the CALPUFF model. Figure 1-1 shows the overall modeling system configuration including the CALMET and CALGRID components.

The above mentioned PUFF/GRID parallel aspect is an important complementary feature in complete impact assessments because CALPUFF excels at estimating primary pollutant concentrations and source culpabilities in the absence of highly non-linear chemistry effects, whereas CALGRID is most reasonable for secondary pollutant species, such as ozone, arising out of highly non-linear chemistry. Such dual modeling approaches are likely to play a greater role in management planning and emissions reduction scenario evaluation as the country moves fully into the post '87 oxidant control strategy milieu.

In the sections which follow we examine the model structure and computer code design and each of the major modules which make up the new CALGRID model. A companion User's Guide contains detailed descriptions of program control files as well as specifications and formats for various input data files.

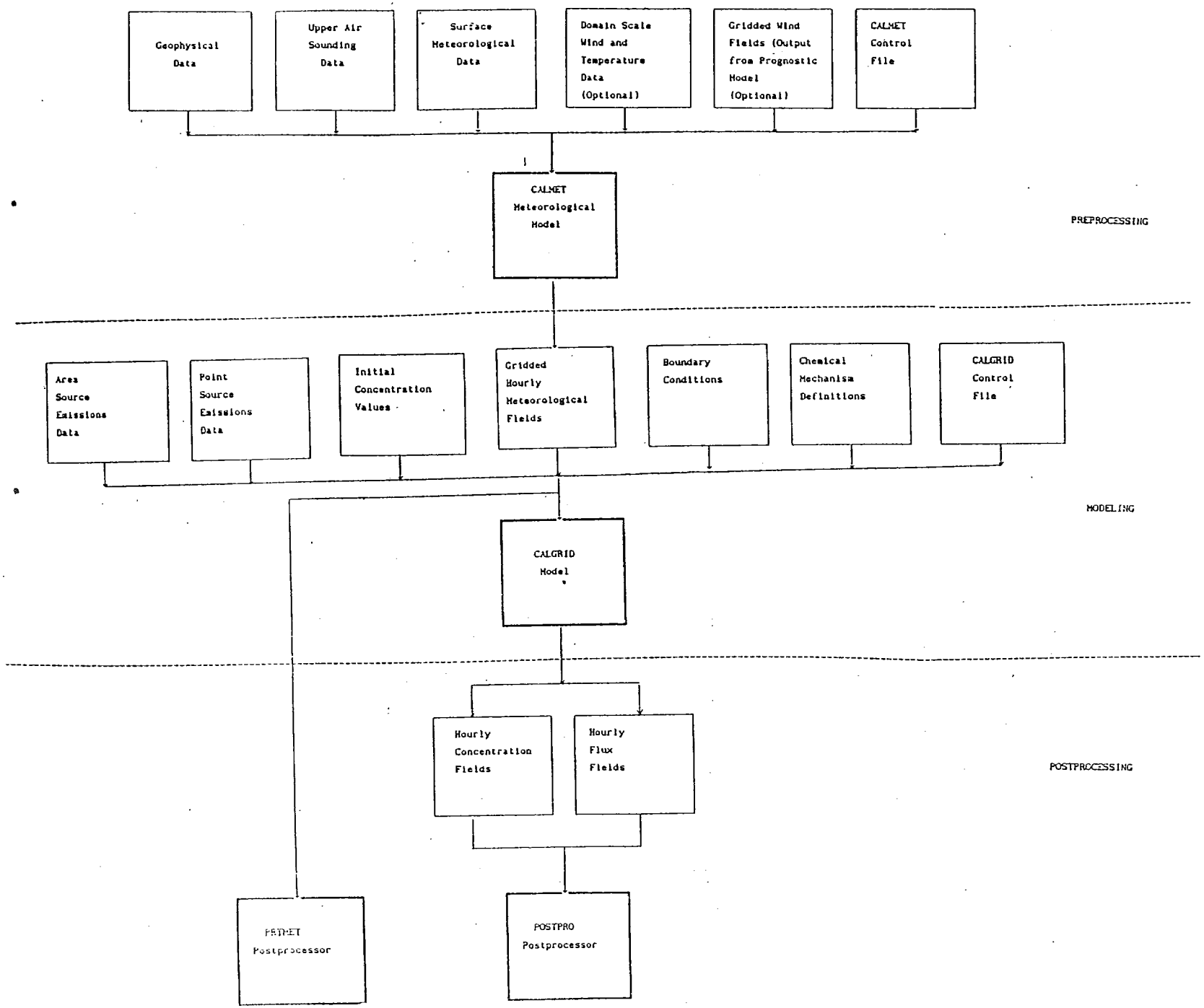

Figure 1-1. Modeling System Flow Diagram.

Section 2

Model Structure and Computer Code Design

The scientific modules which simulate pollutant transport, diffusion, chemical transformation, and removal are incorporated within a model driver module. The model driver determines the structure of the model and overall flow of operations, allocates and partitions central memory, processes the program control file, accesses and delivers the data fields required by each scientific module, and provides for the output and storage of the predicted concentration and flux data.

The structure of the driver module is important in determining the overall flexibility, evolutionary potential, and cost-effectiveness of the model. The structure of the CALGRID model is based on the flexible design used in the Acid Deposition and Oxidant Model (ADOM) (Scire and Yamartino, 1984) including dynamic partitioning of arrays. In this section, the design objectives of the model code are discussed along with some of the major features of the driver module responding to these objectives. Much of this discussion is derived from the referenced ADOM document.

2.1 Design Objectives

The general requirements for the model design can be summarized by the following:

- The model must be designed to possess structural flexibility and internal generality.

- The computer code must make efficient use of central memory and be highly computationally efficient.

- The input modules and file structures must be designed to promote program flexibility, integrity, and reliability.

The driver program and scientific modules are designed to promote flexibility on two levels. The model has a highly modular structure with clear, standardized interfaces between modules. Such a structure has many desirable features, including facilitating independent and simultaneous development of different program units, cost-effective module testing, and increased ease of modification or replacement of individual modules.

In addition to the structural flexibility offered by the modularity of the components, the driver program and scientific modules are written with as much internal generality as is consistent with efficient operation of the code. Internal generality refers to the ability of the code to accommodate a range of different options and input values without the need for code changes. For example, the dry deposition module allows the user to select different levels of sophistication in the deposition parameterization. Simple changes to the control file enable the sensitivity of assumptions of constant, user-input deposition velocities vs. those computed by a full resistance model to be evaluated.

In order to increase potential computational efficiency on high speed vector computers, the compute code has been structured to avoid constructions which inhibit vectorization. Features within inner loops such as subroutine calls, conditionals, I/O statements, indirect addressing of array elements, recursion, and order dependencies have been avoided whenever possible. However, although a vector computer would increase computation speed, the code has been designed to not require the use of a vector computer.

Another feature of the driver program is the use of a memory management scheme that internally partitions central memory to accommodate different values for the number of horizontal grid cells or vertical layers. No restrictions are placed on the individual dimensions of arrays dealing with these variables, except by the Fortran-imposed constraint that the total program memory required not exceed a pre-specified (but easily modifiable) upper limit. The scheme makes use of a "master" array which is internally divided into subarrays only as large as is necessary for the particular control parameters specified for that run.

The third objective of the program design is the enhancement of program integrity and reliability. The input modules and the structure of the data files are designed to allow numerous consistency and cross-referencing checks between the specifications in the control file and the information stored in the input data files. The purpose of these checks is to minimize misapplication of a data set or erroneous specification of input parameters. Of course, the system cannot detect unintended but reasonable combinations of input parameters, but the checks will catch many type of input inconsistencies.

Another feature promoting reliability is the structure of the easy to use and self-documenting control file. Along with the parameter input values, the control file can accommodate an unlimited amount of optional text describing the function, type, valid range, units, and default or recommended values for each input variable. This descriptive information also serves to help eliminate erroneous inputs. Section 2.2 contains a brief description of the control file. A more detailed description is contained in the User's Guide.

2.2 Program Control and Options

The model options are selected and controlled by a set of user-specified inputs contained in a file called the control file. This file is a text file containing all of the information necessary to define a run (e.g., starting date, run length, grid specifications, output options, etc.). The control file is organized into a series of functional groups, including the following:

- User comments and run description
- General run control parameters
- Grid control parameters
- Species list
- Chemical parameters for the dry deposition of gases

- Size parameters for the dry deposition of particles

- Miscellaneous dry deposition parameters

- Output options

The specialized inputs to the chemistry module, including the specification of the chemical mechanism, are contained in separate input data files.

The input module allows considerable flexibility in developing and customizing the control file. An unlimited amount of optional descriptive text (e.g., guidance on recommended input values, units, special assumptions or conditions, etc.) may be inserted anywhere within the control file except between the special delimiter character (!). All text outside the delimiters is treated as a user comment and is ignored by the program. The text within the delimiters is read in a free-type format. A sample control file is provided in the User's Guide.

2.3 Operator Splitting

It must be recognized at the outset that the main objective of the UAM (Reynolds et al., 1979) and the current CALGRID models is the computation of ozone concentrations on typical air basin scales of 50-200 km. The importance of non-linear chemistry forces one to abandon conventional plume and puff models, that invoke superposition and thus imply an underlying linearity, and turn to numerical time marching of a conservation equation at a number of grid points. The most widespread approach involves time-integration of the partial differential equation, known as the advection-diffusion equation, by the method of fractional steps (Yanenko, 1971). The Marchuk (1975) decomposition "factorizes" the time development operator connecting time levels n and n+1 as

$$C^{n+1} = A_x A_y A_z A_c A_c A_z A_y A_x C^n \qquad (2\text{-}1)$$

where A_x, A_y are the horizontal transport and diffusion operators; A_z is the vertical transport, diffusion, source injection, and physical depletion (e.g.,

dry deposition) operator; and A_c is the operator containing all chemical conversion terms. This particular approach is second-order accurate in time due to the cancellation of first-order errors via the alternating forward/reverse operator application and compresses the two back-to-back and time consuming chemical operators into a single operation (i.e., $A_c(\Delta t) = A_c(\Delta t/2)A_c(\Delta t/2)$). While various models implement different nesting of the A_z and A_c operators, the basic structure of Eq. (2-1) should be preserved and serves as a vehicle for developing a highly structured and modular code. In addition, this splitting or factorization of the time development operator for the concentration fields enables each operator to be fashioned using the optimal numerical techniques. Such a decomposition is reasonable only if each suboperator A satisfies the condition $|A - 1| = |\alpha\Delta t| \ll 1$. Thus, the time scale $\tau = 1/\alpha$ of a particular process imposes a size constraint on the basic time step Δt. McRae et al. (1982) recently reviewed this split operator approach and recommended using implicit (rather than explicit) time integration procedures. Although implicit time integration is extremely important for the very "stiff," nonlinear chemical operator A_c connecting the various species C_i, it is only marginally important for the vertical operator A_z and is optional for the advection-diffusion operators A_x and A_y.

Section 3

Numerical Methods for Pollutant Transport

3.1 Horizontal Advection and Diffusion

The advection and diffusion of a concentration field C is described by the partial differential equation (PDE):

$$\frac{\partial C}{\partial t} + \underline{\nabla}\cdot(\underline{V}C) - \underline{\nabla}\cdot(K\underline{\nabla}C) = 0 \qquad (3\text{-}1)$$

where $\underline{V}$ is the vector wind field and K is the diffusivity tensor of rank 2. This PDE has a number of analytic solutions but, within the framework of a grid model, must be solved numerically. The significant role of non-linear processes within a photochemical model is responsible for this need for space discretization or gridding and, because the fields to be advected are known at only a finite number of points, errors develop during the transport process. The process of operator splitting then forces a genuine time discretization into the modeling. Time discretization also introduces errors; however, these are not as bothersome for two reasons. First, reducing the time step Δt increases the computer time proportional to $(\Delta x)^{-1}$, whereas reducing the mesh size Δx increases computer time and the required storage by a factor proportional to $(\Delta x)^{-2}$. Second, because operator splitting already limits the accuracy of the time-marching scheme to second order, efforts to retain higher-order temporal accuracy in individual advection steps have questionable value.

Numerous papers have been written describing the theoretical stability characteristics and actual performance of different advection schemes. Roach (1976) provides an extensive introduction to the subject. Recent intercomparisons of advection schemes (e.g., Long and Pepper (1976, 1981), Pepper et al. (1979), Chock and Dunker (1982), Schere (1983), Yamartino and Scire (1984), Chock (1985), van Eykeren et al. (1987)) are far from unanimous in their conclusion of the best overall scheme, but some consensus is emerging with respect to several considerations including:

- the importance of conducting numerous tests, such as short- and long-wavelength fidelity and moments conservation tests, grid transmission tests, and point source tests, in one and two dimensions. Schemes showing superb fidelity with one test can show disastrous properties in another test.

- the constraint that implementation into a model with non-linear operators (e.g., second-order chemistry) and via operator splitting makes it conceptually difficult, if not impossible, to implement a time marching scheme more sophisticated than Euler (i.e., first order)*.

- progressively higher-order spatial accuracy rapidly encounters a "diminishing returns" plateau if one is limited to Euler time marching.

While a full discussion of the pros and cons of the various schemes would be very lengthy a few comments will illuminate the multitude of considerations.

- The Smolarkiewicz (1984) scheme, currently in use in NCAR's RADM, guarantees non-negative concentrations and performed quite well on his original 100 x 100 grid, but diffusion was found to be comparatively large for this expensive scheme when calculations were done on the standard 33 x 33 grid (where gradients are thus three times larger).

---

* A high-order time marching scheme is possible in the absence of the operator splitting associated with the method of fractional steps. In such a case the whole system of equations would be marched at a rate acceptable to the chemical system and a high spatial-order scheme, such as pseudospectral, would then be very promising. Computing costs would, however, be very large.

- The extremely accurate pseudospectral scheme of Christensen and Prahm (1976) and de Haan (1981) loses most of its superiority over lower spatial-order schemes when troublesome negative concentrations are removed and when Euler time marching is used.

- The second-moment method of Egan and Mahoney (1971) is extremely accurate but requires six times as much storage as other methods. More importantly the use of higher moments in a photochemical model demands that sets of chemical equations be solved for these higher moments in addition to the set solved for the mean concentrations (i.e., the zeroth moments).

- The multidimensional flux-corrected transport (MFCT) schemes of Zalesak (1979) often display excessive diffusion in the crosswind direction and can develop shock waves and other instabilities in the along-wind direction.

We proposed the implementation of either a Chapeau function based scheme (e.g., as used in STEM II or as proposed by Chock (1984)) or a modified cubic spline based scheme (e.g., as developed by Yamartino and Scire (1984) for the ADOM). Both of these schemes enable economical, high-fidelity transport with full mass conservation and complete suppression of negative concentrations. In addition, they are both demonstrably superior to SHASTA (Boris and Book, 1973), Zalesak's MFCT, and Smolarkiewicz's (1984) schemes. The spline based scheme requires about 50% more computer time than the Chapeau function scheme on a uniform grid. This computing time differential grows even larger in the variable layer thickness and grid spacing version required for CALGRID. In addition, some of the features which enhanced the spline scheme's performance were sensitive to properties of the driving wind field. Thus, we have decided to implement the Chapeau function scheme into CALGRID.

3.1.1 Chapeau Function Formulation on an Arbitrary Grid

Both cubic splines and Chapeau functions are fourth-order accurate in space and achieve this accuracy through coupling of local and global

properties of the field. Pepper et al. (1979), Long and Pepper (1981), Carmichael et al. (1980) and McRae (1981) describe and test this Galerkin technique based on simple, triangular chapeau (or hat shaped) basis functions. Expanding both the concentration and velocity fields,

$$C(x,t) = \sum_i \alpha_i(t) e_i(x) \tag{3-2a}$$

and

$$u(x,t) = \sum_i \beta_i(t) e_i(x) \tag{3-2b}$$

in terms of the chapeau basis function $e_i(x)$ defined such that

$$e_i = (x - x_{i-1})/\Delta x_- \text{ for } x_{i-1} \le x \le x_i \quad , \tag{3-3a}$$

$$e_i = (x_{i+1} - x)/\Delta x_+ \text{ for } x_i \le x \le x_{i+1} \quad , \tag{3-3b}$$

and zero elsewhere and where $\Delta x_- = x_i - x_{i-1}$ and $\Delta x_+ = x_{i+1} - x_i$, the advection Equation (3-1) rewritten in flux or mass conserving form and combined with the Galerkin constraint that the residuals of the advection equation be orthogonal to the basis functions on the domain yields the equation set

$$M_{ij} \Delta z_j \frac{d\alpha_j(t)}{dt} + N_{ijk} \beta_j(t) \Delta z_k \alpha_k(t) = 0 \tag{3-4}$$

where Δz_j is the depth of the jth cell,

$$M_{ij} = \int dx \; e_i(x) e_j(x) \tag{3-5a}$$

and,

$$N_{ijk} = \int dx \; e_i(x) \left[e_j(x) \frac{d\, e_k(x)}{dx} + e_k(x) \frac{de_j(x)}{dx} \right]$$

Since the basis functions vanish outside the domain specified in Equation

(3-3), only those integrals for j,k = i-1, i, or i+1 are non-zero. In addition, the symmetry relations $M_{ji} = M_{ij}$ and $N_{ikj} = N_{ijk}$ reduce the number of integrals. The final equation for the time derivative $\frac{d\alpha_i(t)}{dt}$ is just the same as the concentration time derivative, $\frac{dC_i}{dt}$ and, after multiplying by a factor of 6, one obtains

$$\Delta x_- \Delta z_{i-1} \frac{dC_{i-1}}{dt} + 2(\Delta x_- + \Delta x_+)\Delta z_i \frac{dC_i}{dt} + \Delta x_+ \Delta z_{i+1} \frac{dC_{i+1}}{dt}$$

$$- (u_i + 2u_{i-1})\Delta z_{i-1} C_{i-1} + (u_{i+1} - u_{i-1})\Delta z_i C_i$$

$$+ (u_i + 2u_{i+1})\Delta z_{i+1} C_{i+1} = 0 \qquad (3\text{-}6)$$

for interior points on the grid. The equation involving the last grid point N is obtained by using half of the chapeau function but gives the same results as if $\Delta x_+ = 0$, $C_{N+1} = C_N$, and $u_{N+1} = u_N$ were assumed in Equation (3-6).

Equation (3-6) is integrated in time by assuming that the concentrations represent time-step average values:

that is, $\frac{dC_i}{dt} = (C_i^{n+1} - C_i^n)/\Delta t$ and $C_i = (C_i^{n+1} + C_i^n)/2$

where the superscript denotes the time level. The resulting tridiagonal matrix

$$[\Delta x_-/\Delta t - u_{i-1} - u_i/2]\Delta z_{i-1} C_{i-1}^{n+1}$$

$$+ [2(\Delta x_- + \Delta x_+)/\Delta t + (u_{i+1} - u_{i-1})/2]\Delta z_i C_i^{n+1}$$

$$+ [\Delta x_+/\Delta t + u_{i+1} + u_i/2]\Delta z_{i+1} C_{i+1}^{n+1} = [\Delta x_-/\Delta t + u_{i-1} + u_i/2]\Delta z_{i-1} C_{i-1}^{n}$$

$$+ [2(\Delta x_- + \Delta x_+)/\Delta t - (u_{i+1} - u_{i-1})/2]\Delta z_i C_i^{n}$$

$$+ [\Delta x_+/\Delta t - u_{i+1} - u_i/2]\Delta z_{i+1} C_{i+1}^{n} \qquad (3\text{-}7)$$

is then easily solved numerically by Gaussian elimination to give the time advanced concentrations C_i^{n+1}.

It should be noted that Equation (3-7) is for interior points and that the end point forms are obtained by setting

$$\Delta x_- = 0 \quad , \; C_0 = C_1 \quad , \text{ and } u_0 = u_1 \text{ for } i = 1$$

or

$$\Delta x_+ = 0 \quad , \; C_{N+1} = C_N \quad , \text{ and } u_{N+1} = u_N \text{ for } i = N.$$

These constraints also provide the outflow conditions when $C_1 = C_2$ and/or $C_N = C_{N-1}$ is first assumed. Proper inflow is obtained by resetting C_1 and/or C_N to appropriate background values after the particular advection step has been completed. This means that grid points 1 and N can have a semi-active status. However, as the chapeau algorithm must also provide storage for the background concentrations, we do not save the outflow updated values of C_1 or C_N and instead hold these fixed as boundary value concentrations.

3.1.2 Advection Fidelity and Filtering

Unfortunately, the chapeau function method causes a small amount of numerical noise to follow in the wake of an advected distribution and this sometimes leads to unacceptable negative concentrations. Various types of filters that remove the unwanted short wavelength noise are discussed by Pepper et al. (1979) and McRae (1981) and all lead to some degradation of fidelity and/or phase. The simple non-linear filter introduced by Forester (1977) appears particularly attractive as

- it is applied selectively to grid points where it is needed, and
- it is a local solution to the diffusion equation.

Referring now to the solution emerging from the chapeau algorithm as C_i, a single pass of the filter gives concentrations C_i defined for a uniform grid

(McRae, 1981) as

$$C_i' = C_i + K_f[(C_{i+1} - C_i)(\Psi_i + \Psi_{i+1}) - (C_i - C_{i-1})(\Psi_i + \Psi_{i-1})]/2 \quad (3\text{-}8)$$

where $K_f \leq 1/3$ specifies the degree of filtering and $\Psi_i = 1$ or 0 depending on whether filtering at the i^{th} point is desired or not. We have generalized this to an arbitrary grid by re-expressing Eq. (3-8) as

$$C_i' = C_i + K_f[(C_{i+1} - C_i)(\Delta z_{i+1} + \Delta z_i)(\Psi_{i+1} + \Psi_i)\Delta x_+ - (C_i - C_{i-1})(\Delta z_i + \Delta z_{i-1})(\Psi_i + \Psi_{i-1})\Delta x_-]/(4\Delta z_i \Delta x_i) \quad (3\text{-}9)$$

where $\Delta x_i = (x_{i+1} - x_{i-1})/2$ and where further checks ensure that the overall dimensionless diffusivity remains less than one-third and mass is conserved absolutely. While Equation (3-9) is the correct expression of the diffusion equation, it is also found to retard (accelerate) material from entering (leaving) cells having a greatly smaller Δz than their neighbors. This is partially overcome by rewriting terms like $(C_{i+1} - C_i)(\Delta z_{i+1} + \Delta z_i)$ as $2(C_{i+1}\,\Delta z_{i+1} - C_i\,\Delta z_i)$. Such a reformulation still conserves mass and acts as an appropriate filter, though it no longer represents classical diffusion.

Determination of the Ψ_i values is based upon trying to ensure that local extrema in the C_i field are separated by at least $2 \cdot m$ grid cell intervals. This is accomplished by first setting all $\Psi_i = 0$ and defining the sign function

$$S_i = \begin{cases} 1 \text{ if } C_i \geq C_{i-1} \\ 0 \text{ if } C_i < C_{i-1} \end{cases} \quad (3\text{-}10)$$

If $S_i = S_{i+1}$ then the i^{th} point is not an extrema, Ψ_i remains at zero and the next point, i+1, is considered. If $S_i \neq S_{i+1}$ then S_j is checked over the two separate intervals $j = i-m$ to $i-1$ and $j = i+1$ to $i+m+1$ to ensure that there are no additional sign changes in either interval and that the separate

intervals have opposite sign. If this condition is satisfied, one again moves on to i+1; however, if the aforementioned condition is not satisfied then $\Psi_j = 1$ for $j = i-\ell$ to $i+\ell$, when $\ell \leq m$.

In order to filter only the short wavelength noise, $m=\ell=1$ was selected and two full iterations of the filter performed. Experimentally, a K_f of 0.2 was found to prevent negative values under the harshest of initial conditions; however, excessive diffusion occurred for a number of situations. As a compromise, the basic Forester design of $\Psi_j=1$ for $j = i-1$, i, and i+1 was replaced with $\Psi_j = 2$ for $j = i$ only. This retains diffusion at the local extremum without unnecessary satellite diffusion. In addition, the filtering was restricted to minima only (i.e., rather than for both minima and maxima) but extended to include any more global minima where negative concentrations were encountered.

There is also the requirement for explicit diffusion in this modeling process. As will be discussed in a subsequent subsection, this explicit diffusion further damps undesirable ripples and helps eliminate negative concentrations. As diffusion converts short wavelength ripples to longer wavelength ripples, attempts to include explicit diffusion before the Forester-type filter proved counter-productive. It is therefore applied after the determination of the filtered concentrations.

While the above procedures virtually eliminate all occurrences of negative concentrations, they do not absolutely guarantee the absence of negatives. Thus, a final sweep through the concentration array is made. If a negative value is encountered, mass is borrowed first from the lower concentration nearest neighbor with the objective of reducing "drag" on the distribution and its accompanying train of progressively smaller trailing ripples. If there is inadequate mass here, additional borrowing takes place from the other neighbor. Still remaining mass deficits are swept along until a suitable donor cell is found, although in practice, such sweeping is seldon required.

3.1.3 Advection Scheme Performance and Numerical Diffusion

One of the tests routinely done to evaluate advection fidelity of the algorithm including its filter consists of the circular wind field transport of a cosine-hill distribution of concentration, specified as $C = 50\ (1 + \cos \pi R/4)$ with $R^2 = (i - i_o)^2 + (j - j_o)^2$ and (i_o, j_o) being the central grid cell coordinates. Such a test was used extensively by Chock and Dunker (1982) in their comparative study of advection and was carried out on a 33x33 grid with a wind such that the distribution center would lie at a radius of ten grid cells and would complete one full revolution in 240 time steps. Figure 3-1a shows the grid and the initial concentration distribution. Not seen is the varying cell thickness which is allowed to change linearly from 50 m in the upper left to 150 m in the lower right of the grid. Figures 3-1b and 3-1c show the distribution after one and two full counterclockwise revolutions, corresponding to elapsed times of 12 and 24 hours, respectively. It is also worth noting that this test corresponds to an advective speed of 5.8 m/sec, equivalent to a Courant number of 0.262, at the cosine hill peak with maximum speeds reaching 9.3 m/sec (i.e., cfl = 0.42) at the periphery of the grid.

These tests show that after two full revolutions, or 24-hours, the distribution retains 69% of its peak height, exhibits no lags in transport (i.e., the center ended up exactly at its starting point), and except for a small amount of trailing material, shows no serious shape distortion. In a comparable test involving the SHASTA method, Figure 3-2 shows that only 21% of peak height is retained after two revolutions. Thus, the Chapeau function method is far less diffusive than SHASTA in tests of long wavelength (i.e., $\lambda = 8\Delta x$) advection fidelity and has been shown (Yamartino and Scire, 1984) to outperform SHASTA in a wide range of other short and long wavelength advection tests as well.

Figure 3-3 shows the comparable result using an eighth-order, flux-corrected transport (FCT-8) scheme formulated according to procedures described by Zalesak (1979) and very similar to that tested by Schere (1983). While peak height is well preserved, the distribution shows noticeable lag and distortion; however these shortcomings are not very severe and do not show up

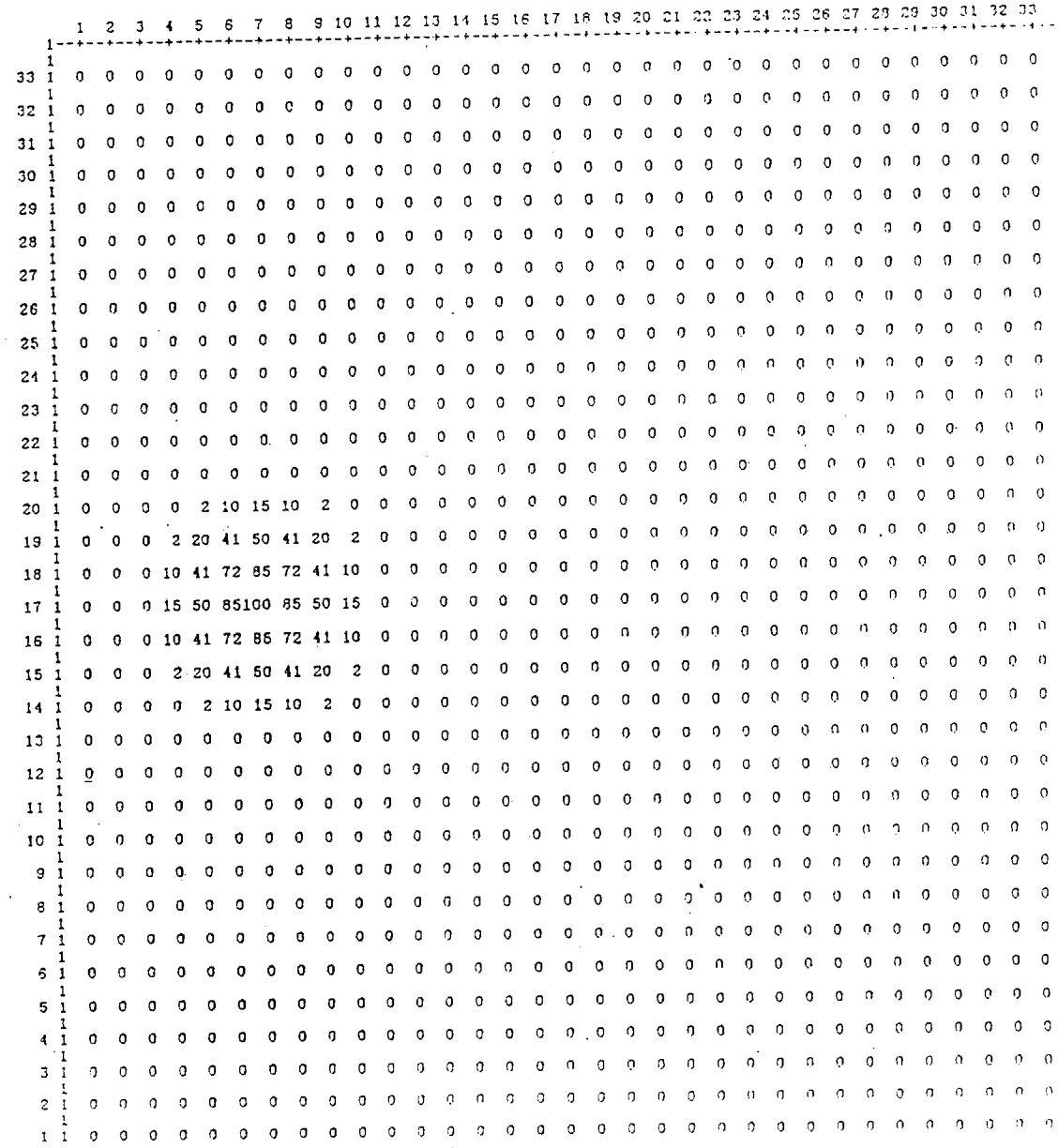

Figure 3-1. Cosine hill rotation test using Chapeau function method. Time steps of 3 Min. and mesh size of 4 km are used. Average and peak Courant numbers are 0.26 and 0.42 respectively.

a) Initial Concentrations

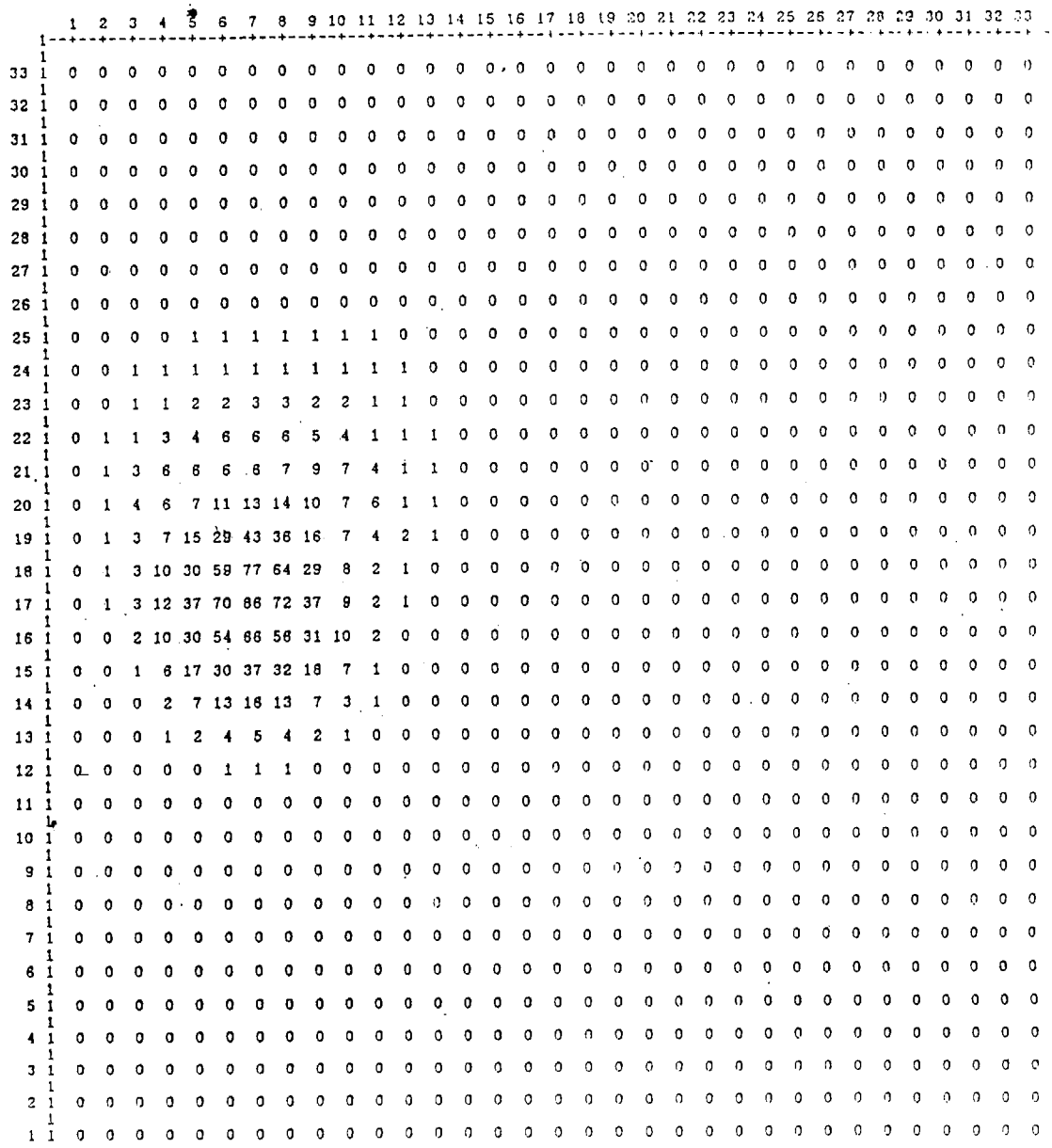

Figure 3-1. Cosine hill rotation test using Chapeau function method.

b) After one full rotation or 240 time steps.

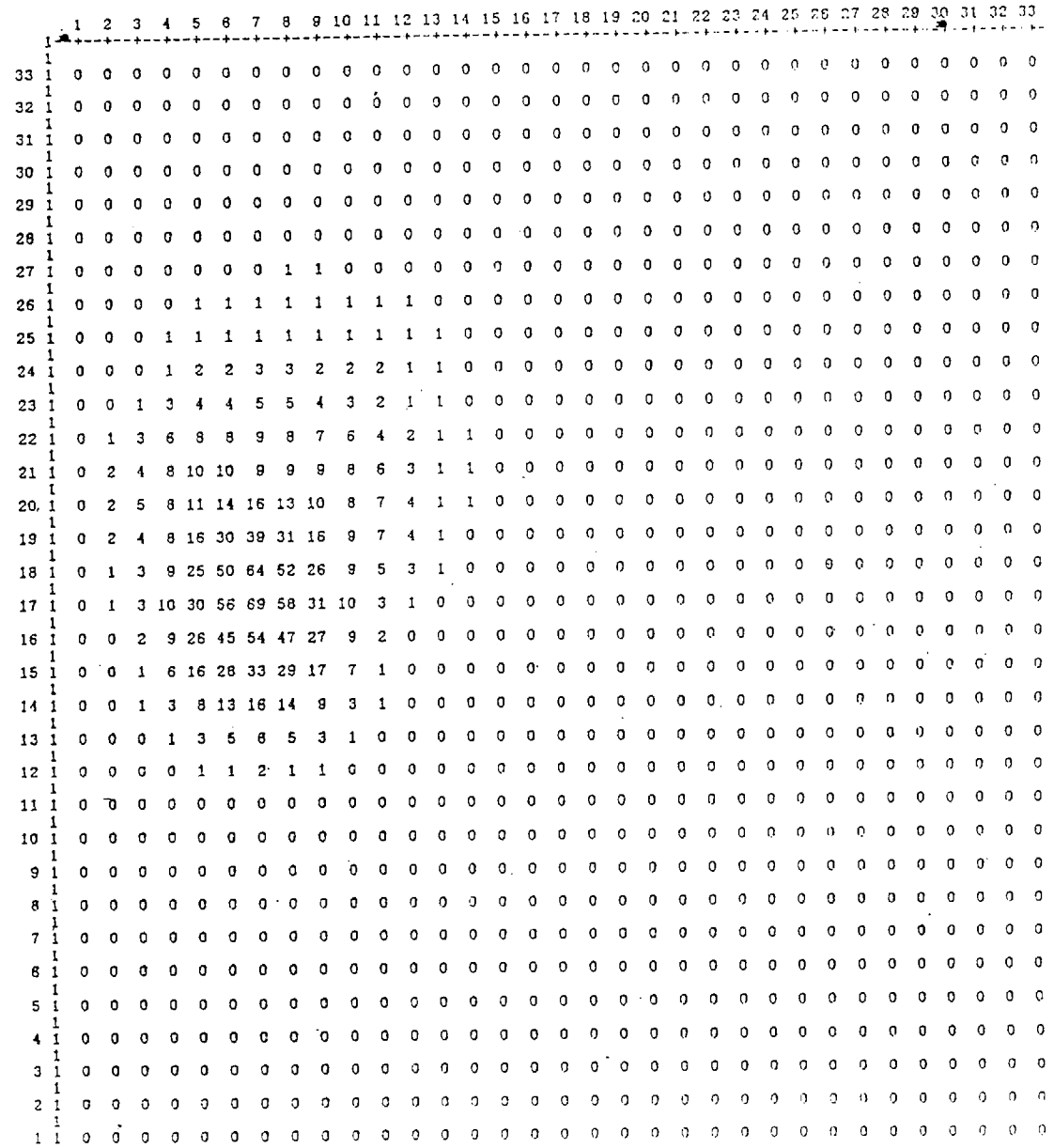

Figure 3-1. Cosine hill rotation test using Chapeau function method.

c) After two full rotations or 480 time steps.

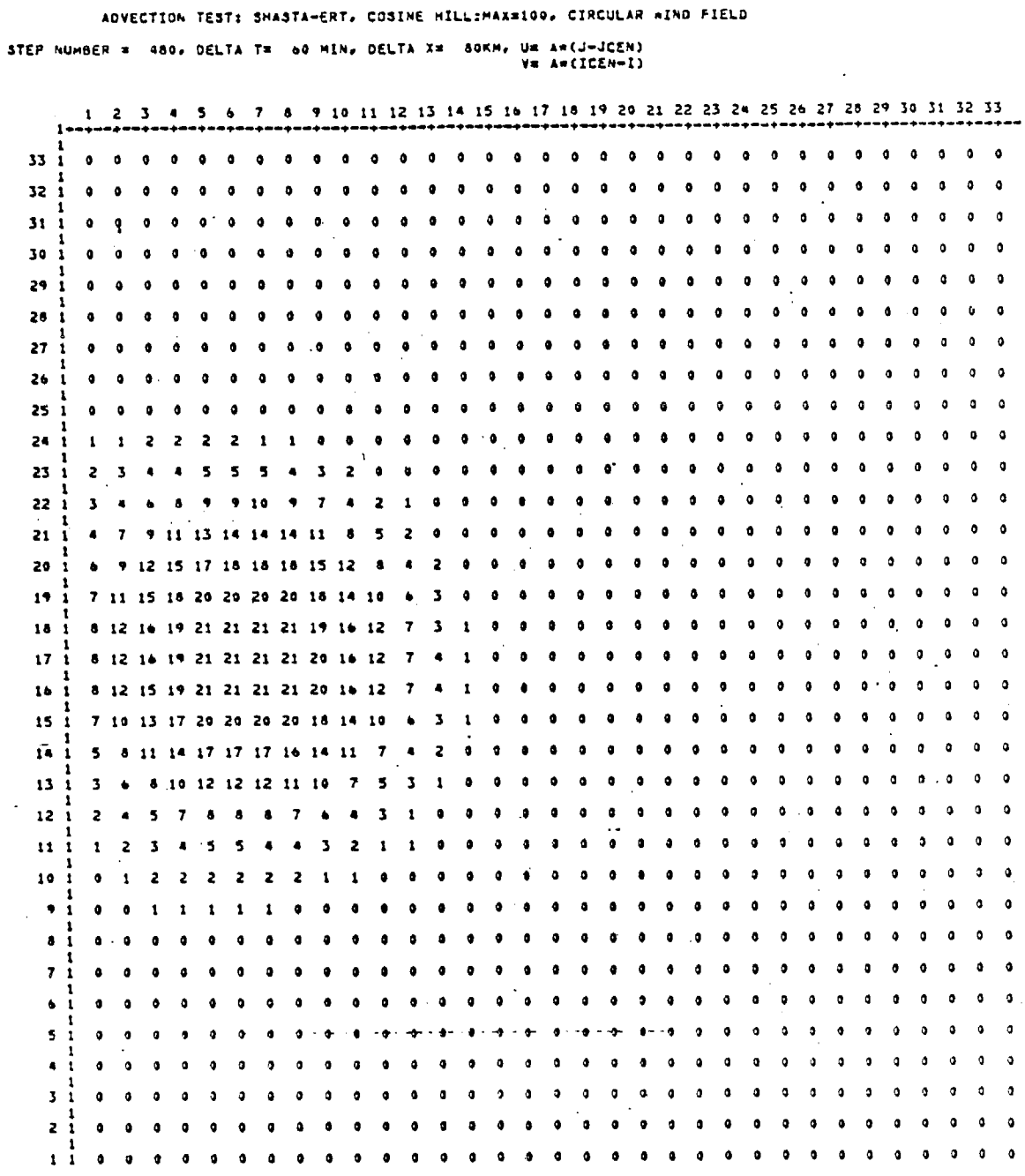

Figure 3-2. Cosine hill rotation test using the SHASTA method. The figure shows the resulting concentration field after two full rotations or 480 time steps. Source: Yamartino and Scire (1984).

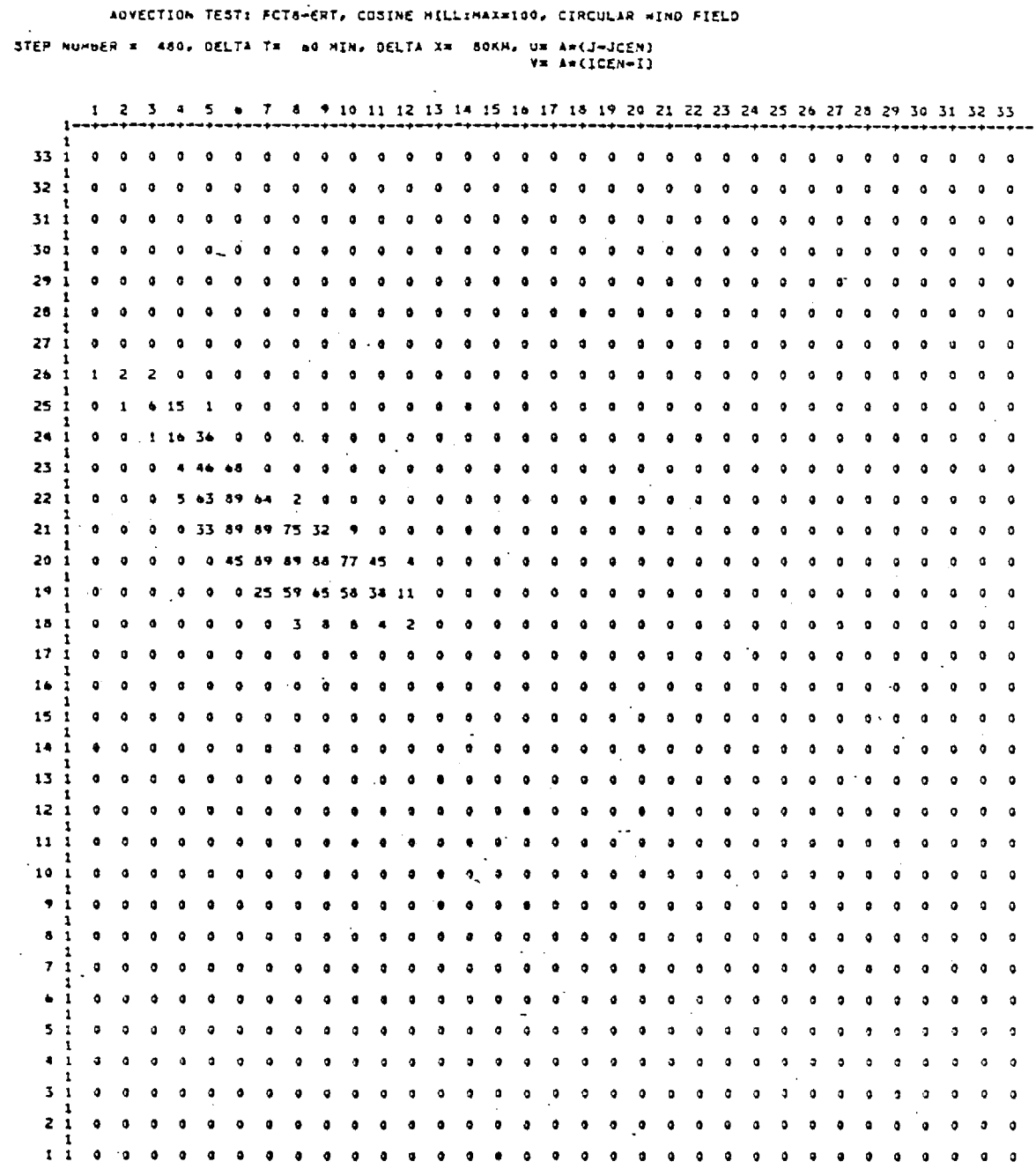

Figure 3-3. Cosine hill rotation test using the FCT-8 method. The figure shows the resulting concentration field after two full rotations or 480 time steps. Source: Yamartino and Scire (1984).

Table 3-1

Cosine Hill Rotation Test

Scheme	C_{Peak}(%)	$\Delta\sigma$(%)	ΣC_i^2(%)	Comment
SHASTA*	21	+ 113.	27.	- Phoenical LPE
FCT-8*	89	+ 27.	110.	- Lag + Distortion
CHAP2D*	69	+ 72.	50.	- Forester Filter
CHAPEAU	69	+ 76. 78.	48. 53.	- Modified Filter, No Zeros

* Source: Yamartino and Scire (1984)

in the cosine hill performance measures summarized in Table 3-1. For the quantities tabulated, the ideal advection scheme would yield a peak concentration of 100% of the original, zero growth in the standard deviation of the spatial distribution, and a sum of squares equal to 100 percent of the original. This latter performance measure was indicated by Chock and Dunker (1982) as being significant in problems involving non-linear chemistry, where bi-linear concentration products are involved.

While the above, long wavelength propagation tests tend to show an advection scheme at its best, adequate short wavelength performance is also extremely important in air quality simulation models and is more difficult to obtain. One of the most stringent tests involves the 2-d transport and diffusion of emissions from a single grid cell point source. Figure 3-4 shows the effect of switching-on a point-source at grid location (7,7) and transporting the plume toward the upper-right corner at Courant numbers of 0.5 in each dimension. Results are displayed for the chapeau function scheme after 20 time steps. Ideally, the centerline concentration plus background should be 1000. Figures 3-5, 3-6, and 3-7 display the corresponding results using the SHASTA, FCT-8, and CHAP2D* schemes respectively. The SHASTA approach is well behaved but quite diffusive, whereas the FCT-8 scheme is unstable and involves bunching of material along the plume axis in a way that leads to spurious maxima and minima. This behavior, also reported by Schere (1983), casts serious doubt on the usefulness of this FCT-8 implementation. Intercomparison of the present chapeau function scheme (Figure 3-4) with the CHAP2D scheme described by Yamartino and Scire (1984) (Figure 3-7) show that the present scheme is less diffusive and exhibits smaller upwind cell disturbances. The normalized concentration values at five grid cells downwind of the source are presented in Table 3-2 and highlight the low numerical diffusion of the current chapeau scheme. Its closest competitor, the CHAP2D scheme, shows 12% smaller values which are, in turn, indicative of 25% higher values of numerical diffusivity.

---

*The more conventional chapeau function plus Forester filter scheme described in Yamartino and Scire (1984).

ADVECTION TEST: CHAPEAU, SINGLE POINT SOURCE, UNIFORM HORIZONTAL WIND

STEP NUMBER = 20, DELTA T= 13 MIN, DELTA X= 10KM, U= 6.25M/S
V= 6.25M/S

LEVEL = 1

	1	2	3	4	5	6	7	8	9	10	11	12	13	14	15	16	17	18	19	20	21	22	23	24	25	26	27	28	29	30
23	50	50	50	50	50	50	50	50	50	50	50	50	50	50	50	50	50	50	50	50	50	50	50	50	50	50	50	50	50	50
22	50	50	50	50	50	50	50	50	50	50	50	50	50	50	50	50	50	50	50	50	50	50	50	50	50	50	50	50	50	50
21	50	50	50	50	50	50	50	50	50	50	50	50	50	50	50	50	50	50	50	50	50	50	50	50	50	50	50	50	50	50
20	50	50	50	50	50	50	50	50	50	50	50	50	50	50	50	50	51	50	50	50	50	50	50	50	50	50	50	50	50	50
19	50	50	50	50	50	50	50	50	50	50	50	50	51	51	53	58	57	54	51	50	50	50	50	50	50	50	50	50	50	50
18	50	50	50	50	50	50	50	50	50	50	51	53	57	62	78	103	88	66	54	50	50	50	50	50	50	50	50	50	50	50
17	50	50	50	50	50	50	50	50	50	52	52	62	74	93	200	232	161	89	58	51	50	50	50	50	50	50	50	50	50	50
16	50	50	50	50	50	50	50	51	51	54	61	86	113	199	448	417	235	105	59	51	50	50	50	50	50	50	50	50	50	50
15	50	50	50	50	50	50	50	50	52	58	70	124	159	498	655	436	201	84	54	51	50	50	50	50	50	50	50	50	50	50
14	50	50	50	50	50	50	51	52	56	62	110	155	474	707	458	197	91	60	52	50	50	50	50	50	50	50	50	50	50	50
13	50	50	50	50	50	50	52	52	70	77	148	480	745	481	215	126	76	55	51	50	50	50	50	50	50	50	50	50	50	50
12	50	50	50	50	50	51	56	59	116	177	390	819	437	133	106	82	59	52	50	50	50	50	50	50	50	50	50	50	50	50
11	50	50	50	50	51	53	67	76	211	422	841	444	147	102	73	59	53	51	50	50	50	50	50	50	50	50	50	50	50	50
10	50	50	50	50	52	57	80	94	536	837	449	155	95	69	57	52	51	50	50	50	50	50	50	50	50	50	50	50	50	50
9	50	50	50	50	52	69	139	427	926	450	119	89	72	56	52	51	50	50	50	50	50	50	50	50	50	50	50	50	50	50
8	50	49	60	51	57	77	428	993	422	150	95	64	57	52	51	50	50	50	50	50	50	50	50	50	50	50	50	50	50	50
7	50	49	50	50	56	60	983	522	158	75	56	56	53	51	50	50	50	50	50	50	50	50	50	50	50	50	50	50	50	50
6	50	50	50	50	50	51	58	80	70	58	52	51	51	50	50	50	50	50	50	50	50	50	50	50	50	50	50	50	50	50
5	50	50	50	50	50	50	56	57	53	52	50	50	50	50	50	50	50	50	50	50	50	50	50	50	50	50	50	50	50	50
4	50	50	50	50	50	50	50	51	50	50	50	50	50	50	50	50	50	50	50	50	50	50	50	50	50	50	50	50	50	50
3	50	50	50	50	50	50	50	50	50	50	50	50	50	50	50	50	50	50	50	50	50	50	50	50	50	50	50	50	50	50
2	50	50	50	50	50	50	50	49	50	50	50	50	50	50	50	50	50	50	50	50	50	50	50	50	50	50	50	50	50	50
1	50	50	50	50	50	50	50	50	50	50	50	50	50	50	50	50	50	50	50	50	50	50	50	50	50	50	50	50	50	50

Figure 3-4. Two-dimensional linear advection of a single-cell point source plume using the CHAPEAU algorithm. The figure shows the concentration pattern after 20 time steps with Courant numbers of +1/2 in the x and y directions. The peak centerline concentrations should be 1000 including the background of 50.

ADVECTION TEST: SHASTA-ENT, SINGLE POINT SOURCE, UNIFORM HORIZ WIND

STEP NUMBER = 20, DELTA T= 13 MIN, DELTA X= 10KM, U= 6.25M/S
V= 6.25M/S

LEVEL = 1

	1	2	3	4	5	6	7	8	9	10	11	12	13	14	15	16	17	18	19	20	21	22	23	24	25	26	27	28	29	30
23	50	50	50	50	50	50	50	50	50	50	50	50	50	50	50	50	50	50	50	50	50	50	50	50	50	50	50	50	50	50
22	50	50	50	50	50	50	50	50	50	50	50	50	50	50	50	50	50	50	50	50	50	50	50	50	50	50	50	50	50	50
21	50	50	50	50	50	50	50	50	50	50	50	50	50	50	50	50	50	50	50	50	50	50	50	50	50	50	50	50	50	50
20	50	50	50	50	50	50	50	50	50	50	50	50	50	50	50	50	50	50	53	53	50	50	50	50	50	50	50	50	50	50
19	50	50	50	50	50	50	50	50	50	50	50	50	50	50	55	70	80	85	72	53	50	50	50	50	50	50	50	50	50	50
18	50	50	50	50	50	50	50	50	50	50	50	50	50	65	133	171	179	157	83	51	50	50	50	50	50	50	50	50	50	50
17	50	50	50	50	50	50	50	50	50	50	50	50	57	156	282	312	290	183	83	50	50	50	50	50	50	50	50	50	50	50
16	50	50	50	50	50	50	50	50	50	50	50	52	145	316	406	387	307	179	72	50	50	50	50	50	50	50	50	50	50	50
15	50	50	50	50	50	50	50	50	50	50	50	131	319	443	441	387	274	128	55	50	50	50	50	50	50	50	50	50	50	50
14	50	50	50	50	50	50	50	50	50	50	114	313	458	470	441	329	164	65	50	50	50	50	50	50	50	50	50	50	50	50
13	50	50	50	50	50	50	50	50	50	91	301	470	486	459	330	162	66	50	50	50	50	50	50	50	50	50	50	50	50	50
12	50	50	50	50	50	50	50	50	73	288	483	504	471	304	125	56	50	50	50	50	50	50	50	50	50	50	50	50	50	50
11	50	50	50	50	50	50	50	60	267	500	528	486	297	108	50	50	50	50	50	50	50	50	50	50	50	50	50	50	50	50
10	50	50	50	50	50	50	50	226	522	563	505	286	95	50	50	50	50	50	50	50	50	50	50	50	50	50	50	50	50	50
9	50	50	50	50	50	50	139	548	619	529	265	82	50	50	50	50	50	50	50	50	50	50	50	50	50	50	50	50	50	50
8	50	50	50	50	50	50	442	774	536	226	63	50	50	50	50	50	50	50	50	50	50	50	50	50	50	50	50	50	50	50
7	50	50	50	50	50	50	842	872	158	50	50	50	50	50	50	50	50	50	50	50	50	50	50	50	50	50	50	50	50	50
6	50	50	50	50	50	50	50	50	50	50	50	50	50	50	50	50	50	50	50	50	50	50	50	50	50	50	50	50	50	50
5	50	50	50	50	50	50	50	50	50	50	50	50	50	50	50	50	50	50	50	50	50	50	50	50	50	50	50	50	50	50
4	50	50	50	50	50	50	50	50	50	50	50	50	50	50	50	50	50	50	50	50	50	50	50	50	50	50	50	50	50	50
3	50	50	50	50	50	50	50	50	50	50	50	50	50	50	50	50	50	50	50	50	50	50	50	50	50	50	50	50	50	50
2	50	50	50	50	50	50	50	50	50	50	50	50	50	50	50	50	50	50	50	50	50	50	50	50	50	50	50	50	50	50
1	50	50	50	50	50	50	50	50	50	50	50	50	50	50	50	50	50	50	50	50	50	50	50	50	50	50	50	50	50	50

Figure 3-5. Two-dimensional linear advection of a single-cell point source plume using the SHASTA algorithm. The figure shows the concentration pattern after 20 time steps with Courant numbers of +1/2 in the x and y directions. The peak centerline concentration should be 1000 including the background of 50. Source: Yamartino and Scire (1984).

ADVECTION TEST: FCTA-ERT, SINGLE POINT SOURCE, UNIFORM HORIZ WIND

STEP NUMBER = 20, DELTA T= 13 MIN, DELTA X= 10KM, U= 6.25M/S
V= 6.25M/S

LEVEL = 1

	1	2	3	4	5	6	7	8	9	10	11	12	13	14	15	16	17	18	19	20	21	22	23	24	25	26	27	28	29	30
23	50	50	50	50	50	50	50	50	50	50	50	50	50	50	50	50	50	50	50	50	50	50	50	50	50	50	50	50	50	50
22	50	50	50	50	50	50	50	50	51	50	50	50	50	50	50	50	50	50	50	50	50	50	50	50	50	50	50	50	50	50
21	50	50	50	50	50	50	50	50	50	57	50	50	50	50	50	50	50	50	50	50	50	50	50	50	50	50	50	50	50	50
20	50	50	50	50	50	50	50	50	50	54	89	50	50	50	50	50	50	50	50	50	50	50	50	50	50	50	50	50	50	50
19	50	50	50	50	50	50	50	50	50	50	79	196	50	50	50	50	50	50	50	50	50	50	50	50	50	50	50	50	50	50
18	50	50	50	50	50	50	50	50	50	50	50	158	426	50	50	50	50	50	50	50	50	50	50	50	50	50	50	50	50	50
17	50	50	50	50	50	50	50	50	50	50	50	50	309	682	158	50	50	50	50	50	50	50	50	50	50	50	50	50	50	50
16	50	50	50	50	50	50	50	50	50	50	50	50	50	477	698	276	50	50	50	50	50	50	50	50	50	50	50	50	50	50
15	50	50	50	50	50	50	50	50	64	50	50	50	50	50	552	698	158	50	50	50	50	50	50	50	50	50	50	50	50	50
14	50	50	50	50	50	50	50	50	51	275	285	154	50	50	50	477	682	50	50	50	50	50	50	50	50	50	50	50	50	50
13	50	50	50	50	50	50	50	50	50	232	693	693	250	50	50	50	309	426	50	50	50	50	50	50	50	50	50	50	50	50
12	50	50	50	50	50	50	50	50	50	50	652	693	693	154	50	50	50	158	196	50	50	50	50	50	50	50	50	50	50	50
11	50	50	50	50	50	50	50	50	152	93	493	652	693	285	50	50	50	50	79	89	50	50	50	50	50	50	50	50	50	50
10	50	50	50	50	50	50	50	221	622	489	93	50	232	275	50	50	50	50	50	54	57	50	50	50	50	50	50	50	50	50
9	50	50	50	50	50	50	79	689	694	622	152	50	50	51	64	50	50	50	50	50	50	51	50	50	50	50	50	50	50	50
8	50	50	50	50	50	50	676	720	689	221	50	50	50	50	50	50	50	50	50	50	50	50	50	50	50	50	50	50	50	50
7	50	50	50	50	50	50	525	676	79	50	50	50	50	50	50	50	50	50	50	50	50	50	50	50	50	50	50	50	50	50
6	50	50	50	50	50	50	50	50	50	50	50	50	50	50	50	50	50	50	50	50	50	50	50	50	50	50	50	50	50	50
5	50	50	50	50	50	50	50	50	50	50	50	50	50	50	50	50	50	50	50	50	50	50	50	50	50	50	50	50	50	50
4	50	50	50	50	50	50	50	50	50	50	50	50	50	50	50	50	50	50	50	50	50	50	50	50	50	50	50	50	50	50
3	50	50	50	50	50	50	50	50	50	50	50	50	50	50	50	50	50	50	50	50	50	50	50	50	50	50	50	50	50	50
2	50	50	50	50	50	50	50	50	50	50	50	50	50	50	50	50	50	50	50	50	50	50	50	50	50	50	50	50	50	50
1	50	50	50	50	50	50	50	50	50	50	50	50	50	50	50	50	50	50	50	50	50	50	50	50	50	50	50	50	50	50

Figure 3-6. Two-dimensional linear advection of a single-cell point source plume using the FCT-8 algorithm. The figure shows the concentration pattern after 20 time steps with Courant numbers of +1/2 in the x and y directions. The peak centerline concentration should be 1000 including the background of 50. Source: Yamartino and Scire (1984).

ADVECTION TEST: CHAP2D-ERT, SINGLE POINT SOURCE, UNIFORM HORIZ WIND

STEP NUMBER = 20, DELTA T= 13 MIN, DELTA X= 10KM, U= 6.25M/S
V= 6.25M/S

LEVEL = 1

	1	2	3	4	5	6	7	8	9	10	11	12	13	14	15	16	17	18	19	20	21	22	23	24	25	26	27	28	29	30
23	50	50	50	50	50	50	50	50	50	50	50	50	50	50	50	50	50	50	50	50	50	50	50	50	50	50	50	50	50	50
22	50	50	50	50	50	50	50	50	50	50	50	50	50	50	50	50	50	50	50	50	50	50	50	50	50	50	50	50	50	50
21	50	50	50	50	50	50	50	50	50	50	50	50	50	50	50	50	50	50	50	50	50	50	50	50	50	50	50	50	50	50
20	50	50	50	50	50	50	50	50	50	50	50	50	50	50	51	52	53	52	51	50	50	50	50	50	50	50	50	50	50	50
19	50	50	50	50	50	50	50	50	50	50	50	51	51	51	57	69	69	60	53	51	50	50	50	50	50	50	50	50	50	50
18	50	50	50	50	50	50	50	50	50	50	51	53	55	59	93	135	121	85	60	52	50	50	50	50	50	50	50	50	50	50
17	50	50	50	50	50	50	50	50	50	51	53	59	63	93	226	289	218	122	69	53	50	50	50	50	50	50	50	50	50	50
16	50	50	50	50	50	50	50	50	51	53	58	63	88	234	461	465	289	136	70	53	50	50	50	50	50	50	50	50	50	50
15	50	50	50	50	50	50	50	50	52	55	65	94	207	484	629	460	229	97	57	51	50	50	50	50	50	50	50	50	50	50
14	50	50	50	50	50	50	50	51	55	62	71	167	502	695	491	225	94	58	52	50	50	50	50	50	50	50	50	50	50	50
13	50	50	50	50	50	50	51	54	58	81	156	502	719	482	206	89	63	55	51	50	50	50	50	50	50	50	50	50	50	50
12	50	50	50	50	50	51	51	61	73	155	525	730	464	177	90	69	56	52	51	50	50	50	50	50	50	50	50	50	50	50
11	50	50	50	50	50	51	57	72	161	504	747	512	193	90	68	57	53	51	50	50	50	50	50	50	50	50	50	50	50	50
10	50	50	50	50	50	56	72	112	538	778	490	158	78	63	54	53	51	50	50	50	50	50	50	50	50	50	50	50	50	5
9	50	50	50	50	54	68	97	512	849	518	164	71	56	53	52	51	50	50	50	50	50	50	50	50	50	50	50	50	50	50
8	50	49	50	51	59	75	503	956	476	149	73	59	55	51	50	50	50	50	50	50	50	50	50	50	50	50	50	50	50	50
7	50	49	50	50	56	60	918	506	119	67	60	52	50	50	50	50	50	50	50	50	50	50	50	50	50	50	50	50	50	50
6	50	50	50	50	50	51	60	76	70	57	51	50	50	50	50	50	50	50	50	50	50	50	50	50	50	50	50	50	50	50
5	50	50	50	50	50	50	56	59	54	51	50	50	50	50	50	50	50	50	50	50	50	50	50	50	50	50	50	50	50	50
4	50	50	50	50	50	50	50	50	50	50	50	50	50	50	50	50	50	50	50	50	50	50	50	50	50	50	50	50	50	50
3	50	50	50	50	50	50	50	50	50	50	50	50	50	50	50	50	50	50	50	50	50	50	50	50	50	50	50	50	50	50
2	50	50	50	50	50	50	49	49	50	50	50	50	50	50	50	50	50	50	50	50	50	50	50	50	50	50	50	50	50	50
1	50	50	50	50	50	50	50	50	50	50	50	50	50	50	50	50	50	50	50	50	50	50	50	50	50	50	50	50	50	50

Figure 3-7. Two-dimensional linear advection of a single-cell point source plume using the CHAP2D algorithm. The figure shows the concentration pattern after 20 time steps with Courant numbers of +1/2 in the x and y directions. The peak centerline concentration should be 1000 including the background of 50. Source: Yamartino and Scire (1984).

Table 3-2

Summary of Results of Point Source Advection Test[+]

Scheme	C(5Δx)/C(Exact)	Comment
SHASTA*	0.504	- Phoenical LPE
FCT-8*	0.693	- Unstable
CHAP2D*	0.730	- Forester Filter
CHAPEAU	0.819	- Modified Filter, No zeros

+ CFL = $\epsilon_x = \epsilon_y = 0.5$

* Source: Yamartino and Scire (1984)

3.1.4 Explicit Horizontal Diffusion

If all $\Psi = 1$ are assumed in Eq. (3-9), one recovers the explicit, finite difference, flux conserving form of the diffusion equation with K_f representing a constant and dimensionless diffusivity, $K_f = K_x \Delta t/(\Delta x)^2$. If the diffusivities, K_x, now vary for each grid point we must generalize Eq. (3-9) one step further to read as

$$C_i' = C_i + \Delta t[(C_{i+1} - C_i)(\Delta z_{i+1} + \Delta z_i)(K_{i+1} + K_i)/\Delta x_+$$

$$- (C_i - C_{i-1})(\Delta z_i + \Delta z_{i-1})(K_i + K_{i-1})/\Delta x_-]/(4\Delta z_i \Delta x_i) \qquad (3\text{-}11)$$

where the subscript x on the K has been dropped. Given that the dimensionless diffusivity or stability parameter, $d = K_x \Delta t/(\Delta x)^2$, seldom exceeds 0.1 for mesoscale flows, we have chosen to use such explicit diffusion. The Euler explicit time marching of diffusion is known (Roach 1976) to be stable in one dimension for $d \leq 1/2$; however, accuracy deteriorates rapidly above $d \approx 1/3$, as this is the value for which a single time step of Equation (3-11) brings a local maximum in cell i into non-oscillatory, steady-state equilibrium with neighbors i-1 and i+1. Thus, given the expected range of and uncertainties in lateral diffusivities, use of the simple Euler time marching imposes no realistic limitations on the model. However, to maintain complete module generality, the maximum value of d is checked as the one-dimensional, advection-diffusion operator sequence is begun. Values of $d > 0.3$ force the entire operator to run at a sub-multiple time step, as is also the case should any Courant number exceed 1.0.

3.2 Vertical Level Scheme and Transport

3.2.1 Vertical Level Scheme and Associated Compensations

In order to retain maximum flexibility we have designed the modeling system to operate in terrain following coordinates

$$Z = z - h(x,y) \qquad (3\text{-}12)$$

In such a system with a compatible meteorological driver, vertical winds are presented in their coordinate adjusted form,

$$W = w - u\frac{\partial h}{\partial x} - v\frac{\partial h}{\partial y} \quad , \tag{3-13}$$

where the w represent the physical, vertical winds in coordinate space.

As it is also desired to make most efficient use of the levels, we retain the flexibilities that the level heights may arbitrarily change in space and time. The main problem with such a system, where the top of level j is located at

$$z_j(x,y,t) = Z_j(x,y,t) + h(x,y) \quad , \tag{3-14}$$

is that the pseudo vertical velocities involved (i.e., $\frac{\partial z_j}{\partial t} = \frac{\partial Z_j}{\partial t}$ and the non-terrain following terms $u\frac{\partial Z_j}{\partial x}$, $v\frac{\partial Z_j}{\partial y}$) can be large with respect to the real winds, w, and the terrain following counterparts, W. This means that a large fraction of the flux being forced through a particular interface is just to accommodate the coordinate system. This is undesirable because numerical diffusion is roughly proportional to the amount of flux exchanged so that the effect of the desired W might easily be lost in the numerical noise. In addition, if lateral advection by the component u brings no new mass of species k into cell j, then application of a corrective vertical velocity $u\frac{\partial Z_j}{\partial x}$ is inappropriate. To mitigate this problem we have adopted two strategies:

1) replacing continuous level movement with mass conserving interpolation onto the new set of levels after the vertical transport step is complete and

2) compensating for spatial gradient terms, $u\frac{\partial Z_j}{\partial x}$ and $v\frac{\partial Z_j}{\partial y}$, just after the horizontal advection step and on a species-by-species basis by tracking horizontal advective fluxes and computing their correct vertical re-apportionment.

While the first of these strategies involves a partial swap of interpolation error for numerical diffusion error for material being moved across one interface, there is a distinct improvement (i.e., reduced numerical diffusion) with the interpolation scheme over advective transport when multiple z-level interfaces are crossed. In addition, the second strategy represents a definite improvement with 2-d horizontal advection, as the methodology recognizes which dimension (i.e., x or y) contributed to the flux excess of a given species rather than using a directionally blind and species blind vertical velocity equal to $-\left(u\frac{\partial Z_j}{\partial x} + v\frac{\partial Z_j}{\partial y}\right)$. This pollutant mass shuffling scheme computes mass transport and excess in each cell via horizontal advection estimates of the interfacial fluxes and then re-apportions the excess into the correct neighboring vertical cells.

Both of the above strategies depend on the definition of a simple matrix $f_{j,j'}$, describing the fractional portion of beginning level j which overlaps, or end up in, the ending level j'. Defined in simple geometrical terms (i.e., lengths) for a system of NZ levels, this transfer matrix is normalized such that

$$\sum_{j=1}^{NZ} f_{j,j'} = 1 \text{ for all } j', \tag{3-15}$$

and therefore is not unlike the matrix encountered in the transilient turbulence theory of Stull (1984). Thus, the mass conserving process of interpolation from a set of levels j onto a new set of vertical levels j' leads to the concentrations, $C_{j'}$, defined as

$$C_{j'} = \sum_{j} f_{j,j'} \cdot C_j \quad , \tag{3-16}$$

whereas the corresponding re-apportionment of a flux F_j, horizontally advected from a column having levels j into a column having levels j' is given as

$$C'_{j'} = C_{j'} + \sum_{j} [f_{j,j'} - \delta_{j,j'} \cdot \Delta z_j/\Delta z_{j'}] \cdot F_j \cdot \Delta t/(\Delta x_j, \Delta z_j) \quad , \qquad (3\text{-}17)$$

where $\delta_{j,j'}$ is the unit matrix, Δz_j and $\Delta z_{j'}$ are the level depths, and Δx_j is the length of the cell j' in the direction of the flux.

It should be noted that whereas Eq. (3-7) will correctly advect the conserved scalar $c_i \Delta z_i$ on a horizontal grid, the subsequent re-apportioning of material between vertical levels by Eq. (3-17) disturbs the initial conditions for the next advection step. This can be compensated for somewhat by appropriate Δz_i weighting of the u_i in Eq. (3-7); however, the net effect of re-distributing a high-order flux, F_j, is to introduce some noise on the grid. For example, an initial uniform concentration field of C = 1.0 advected through a region of five-fold variation in Δz_i will exhibit a "noise" standard deviation of about 0.05 or 5%. Efforts are continuing to reduce this noise level further.

Finally, we note that while the formulations above will work with an arbitrary level definition scheme, CALGRID is equipped with a two-parameter scheme which establishes a near "log-like" spacing of NZ levels while retaining the features that:

- the top of level 1 (i.e., face height z_2) can be held at a fixed height above terrain to facilitate the z-profiling needed in the dry deposition module and consistent use of surface winds;

- an arbitrary number of levels above (NZA) and below (NZB) an arbitrary "diffbreak" face height, z_d, may be specified; and

- the scheme is analytic in z so that optimal grid point heights can be used in the vertical transport equations described in the next section.

The method used to establish this grid involves a succession of transformations. First the full domain of the grid, from the bottom face

position, z_b, to the model domain top face position, z_t, is mapped onto the s interval zero to one via the relation

$$s = [(z-z_b)/(z_t-z_b)] \quad , \tag{3-18}$$

The variable s is then transformed to the variable r,

$$r = \log [1 + (e-1)s] \quad , \tag{3-19}$$

also defined in the domain of zero to one, but designed to give the desired "log-like" spacing. The final transformation to ρ coordinates as

$$\rho = r [(1 + p_1 + p_2)/(1 + p_1 \cdot r + p_2 \cdot r^2)] \tag{3-20}$$

where the two-parameters p_1 and p_2 are chosen to yield the correspondence between face heights z_2 and z_d and ρ values of 1/NZ and (NZB + 1)/NZ, respectively.

3.2.2 Vertical Transport

In contrast to lateral diffusion, vertical diffusion generally dominates the vertical transport step and greater care must be exercised in selecting a numerical scheme. Numerical integration of the vertical diffusion equation is inherently more noisy because (1) variable mesh spacing is generally used to resolve concentration gradients, (2) $(\Delta z)^2/K_z$ can be quite small compared with the time step, and (3) the source emissions terms can act as a strong forcing function, particularly in the shallow surface cell.

The generalized, conservative, finite difference form of Equation (3-1) is

$$C_j^{n+1} = C_j^n + [\gamma(F_{j-1/2}^{n+1} - F_{j+1/2}^{n+1}) + (1-\gamma)(F_{j-1/2}^n - F_{j+1/2}^n)]\Delta t/\Delta z_j$$

$$+ (Q_j - S_j)\Delta t \qquad (3\text{-}21)$$

where

$$F_{j\pm1/2}^n = W_{j\pm1/2}\, C_{j\pm1/2}^n - K_{j\pm1/2} D_{j\pm1/2}^n$$

$$F_{j\pm1/2}^{n+1} = W_{j\pm1/2}\, C_{j\pm1/2}^{n+1} - K_{j\pm1/2} D_{j\pm1/2}^{n+1} \qquad (3\text{-}22)$$

are the fluxes (i.e., ignoring the column constant, cell face area $\Delta x \cdot \Delta y$), including an advective component, at time steps n and n+1, and $C_{j+1/2}$ and $D_{j+1/2}$ are the concentrations and spatial derivatives of the concentrations respectively at the cell faces. As before, Δz_j is the thickness of level j and $\delta z_{j+1/2} = (\Delta z_{j+1} + \Delta z_j)/2$ will be used to denote the distance between grid points. The quantities, Q_j, S_j, vertical diffusivities $K_{j\pm1/2}$, and vertical velocities $W_{j\pm1/2}$ are without temporal superscripts and are, for simplicity, assumed either as constants over the period Δt or as the values appropriate at the mid-point time $(n+1/2)\Delta t$. The parameter γ controls the admixture of present and time advanced quantities and can be varied from zero (explicit time marching) to one-half (Crank-Nicolson method) to one (fully implicit time marching) depending on stability and accuracy considerations.

The degree of spatial accuracy retained by Equation (3-22) is now just a function of the degree of spatial accuracy used in obtaining the cell interface values of $C_{j+1/2}$ and $D_{j+1/2}$ for Equation (3-22) determination of the fluxes. In the first-order approximation

$$C_{j+1/2} = a_{j+1/2} C_j + (1-a_{j+1/2}) C_{j+1} \qquad (3\text{-}23a)$$

and $$D_{j+1/2} = (C_{j+1} - C_j)/\delta z_{j+1/2} \quad , \qquad (3\text{-}23b)$$

where $$a_{j+1/2} = \Delta z_{j+1}/(\Delta z_j + \Delta z_{j+1}) \qquad (3\text{-}23c)$$

Errors are found to be lowest (Roache 1976) when the Δz_j are uniform, which is definitely not the case in most multi-layer, atmospheric pollution models. Thus, the algorithm checks whether the levels are more nearly equal in a linear or transformed (logarithmic) coordinate frame defined by the analytic transformation

$$\rho = f(z) \tag{3-24}$$

such as specified by Equations (3-18) thru (3-20).

In such a transformed system, Eqs. (3-23) are modified by redefining

$$a_{j+1/2} = \Delta\rho_{j+1}/(\Delta\rho_j + \Delta\rho_{j+1})$$

where $\Delta\rho_j = \rho_{j+1/2} - \rho_{j-1/2}$, specifies the ρ depth of layer j, and $\delta z_{j+1/2}$ in Equation (3-23b) is redefined as

$$\delta z_{j+1/2} = \delta\rho_{j+1/2}/(d\rho/dz)_{j+1/2} \quad ,$$

where $\delta\rho_{j+1/2} = (\Delta\rho_j + \Delta\rho_{j+1})/2$ and $d\rho/dz\big|_{j+1/2}$ is the analytic derivative of Equation (3-24) evaluated at $z = z_{j+1/2}$. No other changes to the formalism are required and evaluation on the equal $\Delta\rho$ spacing grid shows that the transformation reduces to $a_{j+1/2} = 1/2$ and only somewhat modified values of $\delta z_{j+1/2}$. In practice, however, donor cell values of $a_{j+1/2}$ (i.e., a=0,1) are used to prevent instabilities and ensure positive concentrations.

Boundary conditions are also quite easily imposed in either the z or ρ coordinate frames. The model allows for diffusive and/or advective interaction with a presumed concentration boundary value above the top of the modeling domain. Designating this concentration as C_{N+1}, Equations (3-22) and (3-23) are used exactly as before provided $K_{N+1/2}$ is specified and

$$a_{N+1/2} = \begin{cases} 0 \text{ for } W_{N+1/2} < 0 \\ 1 \text{ for } W_{N+1/2} \geq 0 \end{cases} .$$

A consistent set of lower boundary conditions are obtained by choosing

$$K_{1/2} = 0 \quad ,$$
$$a_{1/2} = 0 \quad , \text{ and}$$
$$W_{1/2} = -v_d \ ,$$

where v_d is the deposition velocity as described in detail in Section 5 of this report. While it is perhaps somewhat unusual to model dry deposition through an advective boundary condition, the atmospheric resistance component of v_d already involves an integral average over the lowest layer so that the dry flux F_d is indeed

$$F_d = -F_{1/2} = v_d C_1 \tag{3-25}$$

Equation (3-21) can be solved once using the full time step Δt (typically 10-20 minutes) or may be iteratively solved in M steps of duration $\Delta t/M$ for greater solution accuracy in either Crank-Nicolson or fully implicit modes. We have found that a hybrid time differencing scheme, which uses the Crank-Nicolson method when K_z is small or moderate, and the fully implicit method when K_z is large, is more accurate than the fully implicit method alone. Deciding how large to allow M to become, in order to keep the maximum stability, $K_z \Delta t/(\Delta z)^2$, below the cutoff value of 1/2 frequently assumed for Crank-Nicolson integration, thus involves a computing cost versus accuracy tradeoff, as it costs virtually the same to perform M iterations with $\gamma = 1/2$ as with
$\gamma = 1$.

Section 4

Horizontal and Vertical Diffusivity

Nearly all photochemical dispersion models in use today account for non-advective pollutant fluxes through simplified, K-theory closure; that is, through the specification of diagonal tensor terms $K_{xx}(x,y) = K_{yy}(x,y)$ and $K_{zz}(x,y)$ and the neglect of off-diagonal terms (e.g., K_{xz}, K_{yz}). In this section, revised formulas for the K_{yy} and K_{zz} terms are proposed.

4.1 Horizontal Diffusion

In the UAM, the lateral sub-grid scale diffusion process is greatly simplified by assuming a space independent $K_{xx} = K_{yy} = K_H$ of 50 m^2/sec. Conversion of this diffusivity to a non-dimensional atmospheric value of $K_a = K_H \Delta t/(\Delta x)^2$ yields a $K_a = 0.0025$ for $\Delta x = 2$ km and $\Delta t = 200$ sec, but this value must be compared to the effective numerical diffusivity, $K_e \simeq 0.2$, of the SHASTA advection scheme (Boris and Book, 1973) for sharply peaked distributions. Thus, except for very broad, smooth concentration structures on the grid, inclusion of the lateral diffusion process in UAM was purely "cosmetic". While the replacement advection scheme for CALGRID will reduce this worst case K_e/K_a ratio of nearly 100 by a factor of about five, the desirable situation where $K_e \ll K_a$ for all dispersion conditions will still not be fully achieved. Despite this problem, yet in light of its presence, we have implemented several, user-selectable lateral diffusivity formulations.

In order to account for diffusion due to distortion or stress in the horizontal wind field, CALGRID contains the moderately simple Smagorinsky (1963) formulation

$$K_a = \alpha_o^2 |D| \Delta t \qquad (4\text{-}1)$$

where $\alpha_o \simeq 0.28$ and

$$|D| = \left[\left(\frac{\partial v}{\partial x} + \frac{\partial u}{\partial y}\right)^2 + \left(\frac{\partial u}{\partial x} - \frac{\partial v}{\partial y}\right)^2\right]^{1/2} \qquad (4\text{-}2)$$

characterizes the stress in the wind field and can be computed directly from the already existing u, v horizontal wind field components.

Equations (4-1) and (4-2) will, of course, yield diffusivities of zero for a uniform wind field and thus does not account for grid-scale turbulent processes. For plumes which are several kilometers or more across (i.e., Δx or greater), the Briggs (1973) parameterizations of lateral diffusion permit one to extract diffusivities which are constants times the transport wind speed u, (or more properly $(u^2 + v^2)^{1/2}$). These extracted constants are presented in Table 4-1 for both the "urban" and "rural" dispersion growth laws included in the U.S. EPA short range regulatory models. Along with these values, we include a series of "rounded" values which increase by a factor-of-two per stability class as one proceeds from stable (F) thru unstable (A). Given that the short-wavelength numerical diffusivity of the current chapeau function transport scheme is about $30 \cdot u$ (m^2/sec), one would conclude that E and F lateral diffusive transport cannot be realistically simulated, as these diffusivities are below the threshold of existing numerical diffusion. Subtracting a rounded numerical diffusivity values of 32 u from the "rounded" values yields the final column of "suggested" values which a user may input via the CALGRID control file. The user may also select whether the wind field stress induced diffusivity is to be added in to yield a total diffusivity. The lateral diffusion process is then computed explicitly as part of the horizontal transport operator.

Fortunately, the problem of numerical diffusion is not as serious for the vertical direction and permits a more sophisticated treatment.

4.2 Vertical Diffusion

The vertical dispersion coefficients in UAM were developed in the mid-1970's. However, as Wyngaard (1985, 1988) points out, a "revolution" in boundary layer knowledge has taken place since that time. The algorithms in

Table 4-1

Lateral "Grid-Scale" Diffusivities

Diffusivity (m^2/sec)/u(m/sec)

Class	"Urban"*	"Rural"*	"Rounded"**	"Suggested"
A	128	242	256	224
B	128	128	128	96
C	60.5	60.5	64	32
D	32	32	32	0
E	15.1	18	16	0
F	15.1	8	8	0

* Extracted from Briggs (1973) dispersion curves as presented in U.S. EPA (1987)

** Based on a computed numerical diffusivity of about 30·u (m^2/sec) (for ΔX = 2km, Δt = 1800s) for distributions covering more than 3 grid cells.

CALGRID are updated to reflect current knowledge of convective scaling in the daytime boundary layer and local or z-less scaling in the nighttime boundary layer.

Figures 4-1 and 4-2 summarize in a qualitative way our knowledge of scaling laws that apply to the convective and stable boundary layers (the "neutral" boundary layer is merely an asymptotic limit on these figures). In both figures the scaled height, z/h, is used as the ordinate, and stability parameter, h/L, is used as the abscissa. The various parameters are defined in the following ways:

h (m): mixing depth

z (m): elevation above ground

$\tau = \rho u_*^2$ (kg/m sec^2): local momentum flux (positive downward)

u_*(m/s): friction velocity

$\overline{w\theta}$(°Km/s): local sensible heat flux (positive upward)

subscript o: refers to the surface value

$L(m) = -(u_{*o}^3/0.4)/\ (g/T)\overline{w\theta}$: Monin-Obukhov length, defined using surface fluxes

$\Lambda(m) = -\left[(\tau/\rho)^{3/2}/0.4\right]/\ (g/T)\overline{w\theta}$: local Monin-Obukhov length, defined using local fluxes

The boundaries dividing regions on the figures are based on a combination of dimensional analysis, boundary layer theory, and observations.

The revised K_z formulations for CALGRID are defined for each of the regions in Figures 4-1 and 4-2. In addition, K_z formulations are suggested

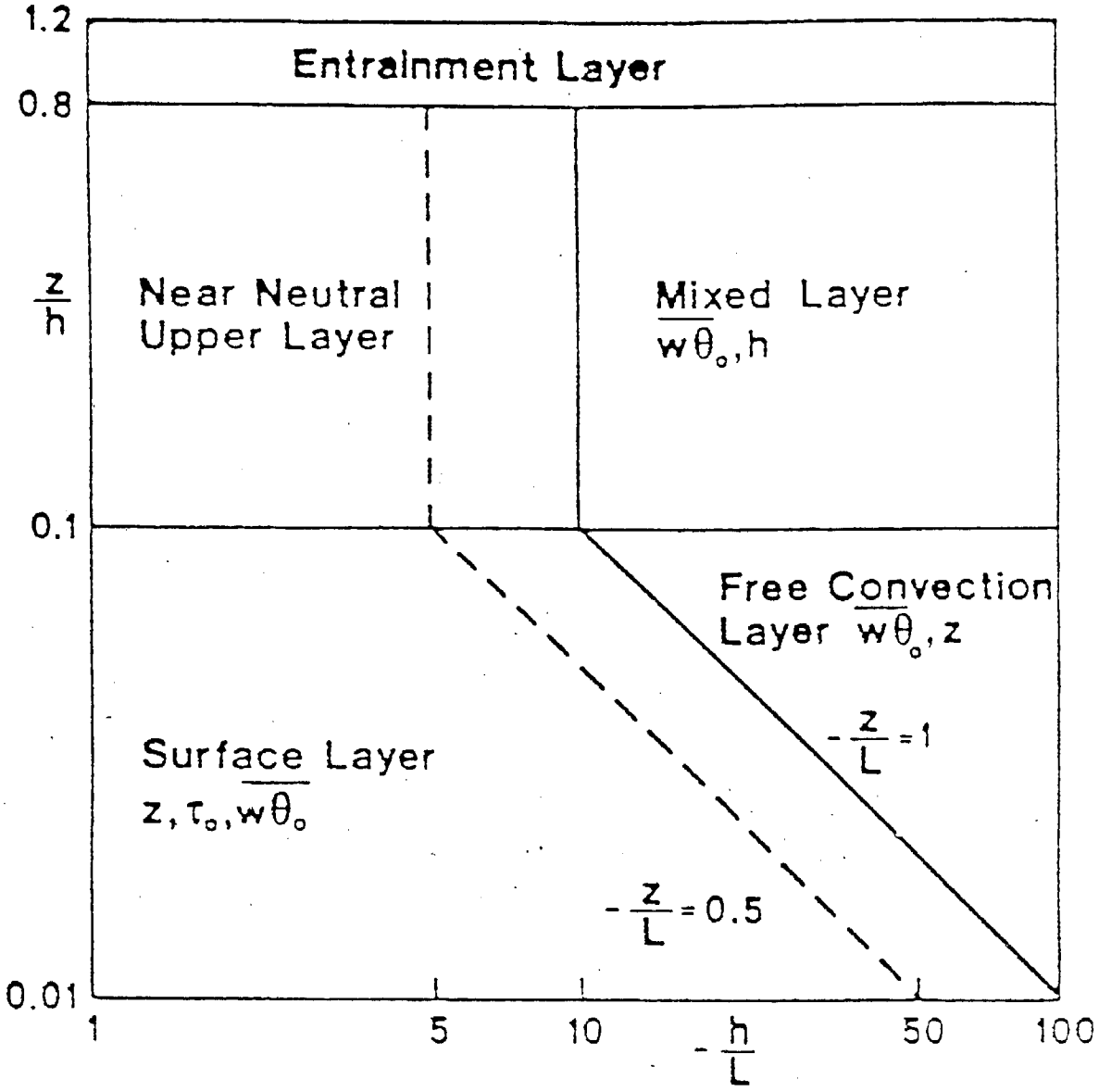

Figure 4-1. Scaling Laws in the Convective Boundary Layer (from Holtslag and Nieuwstadt, 1986).

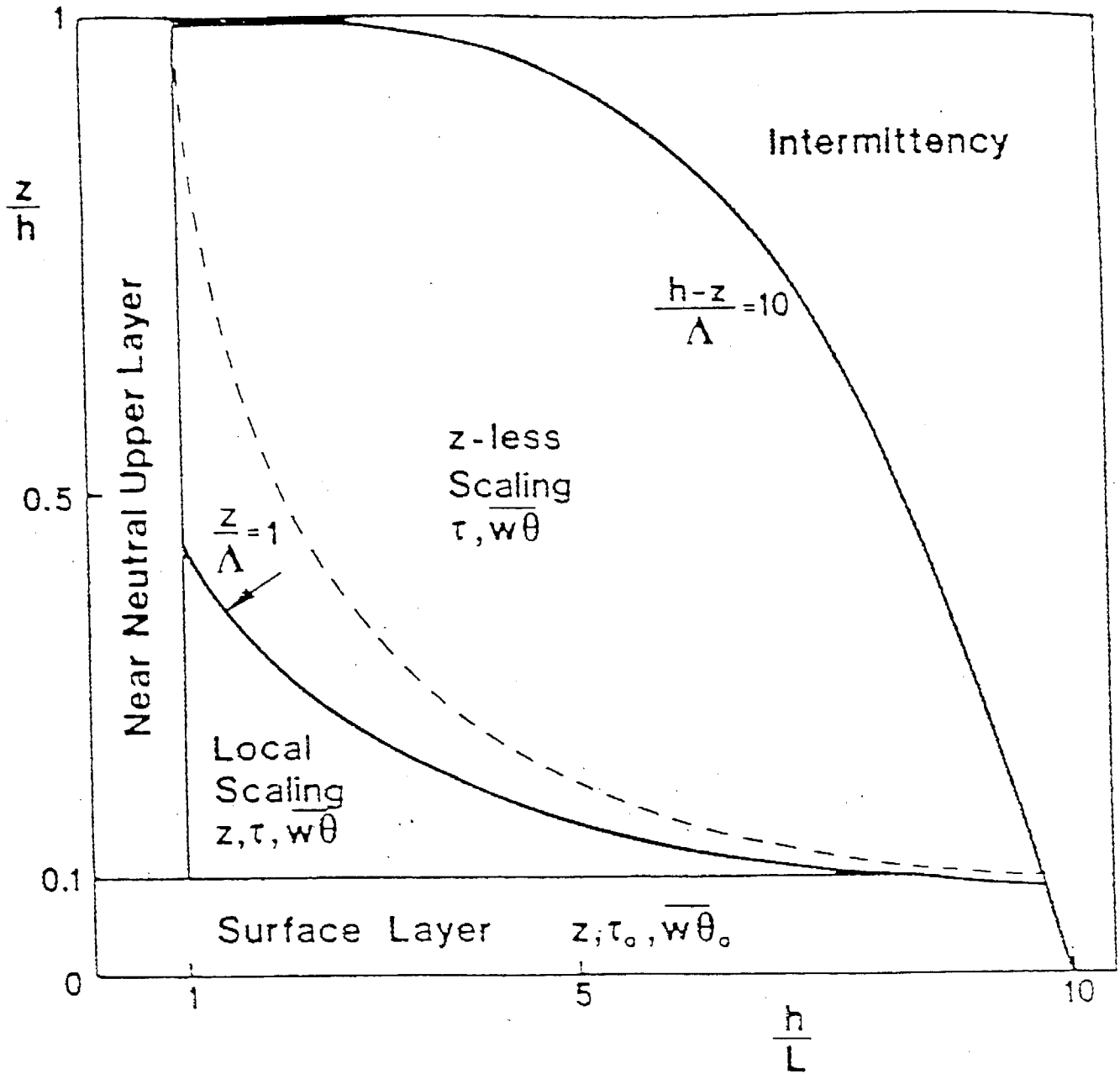

Figure 4-2. Scaling Laws in the Stable Boundary Layer (from Holtslag and Nieuwstadt, 1986).

for the regions above the tops of the figures, where $z/h > 1$. During the nighttime, when the mixing depth is often less than 100 m, it is important to be able to specify K_z at heights above 100 m. The following sections contain contain the proposed K_z formulas. The necessary values of h, τ_o, or u_{o*}, $\overline{w\theta}_o$, and hence L are made available by the CALMET meteorological preprocessor.

Convective Boundary Layer (L < 0)

Surface layer ($z/h \leq 0.1$; $- z/L < 1.0$)

$$K_z = 0.4 u_{o*} z/\phi_h(z/L) \tag{4-3}$$

$$\text{where } \phi_h(z/L) = 0.74(1 - 9z/L)^{-1/2} \tag{4-4}$$

Free Convection Layer ($z/h \leq 0.1$; $- z/L > 1$)

$$K_z = w_* z \tag{4-5}$$

Nearly-neutral upper layer ($0.1 < z/h \leq 1$, $- h/L < 10$)

$$K_z = 0.04 u_{o*} h/\phi_h(0.1h/L) \tag{4-6}$$

(i.e., K_z from Eq. (4-3) is evaluated at $z/h = 0.1$)

where the convective velocity scale is given by:

$$w_* = (gh\ \overline{w\theta}_o/T)^{1/3} \tag{4-7}$$

Mixed layer ($0.1 < z/h \leq 1.0$; $- h/L > 10$)

$$K_z = 0.1\ w_* h \tag{4-8}$$

Layer above h ($z/h > 1.0$)

K_z = 0.1 * (K_z at top of near-neutral upper layer (Eq. 4-6) or mixed layer (Eq. 4-8)) (4-9)

Stable Boundary Layer (L > 0)

Surface layer ($z/h \leq 0.1$; $(h - z)/\Lambda < 10$)

$$K_z = 0.4u_* z/\phi_h(z/L) \tag{4-10}$$

where $\phi_h(z/L) = 0.74 + 4.7z/L$ (4-11)

Near neutral upper layer ($0.1 < z/h < 1.0$; $h/L < 1$)

$$K_z = 0.04u_{o*} h/\phi_h(0.1h/L) \tag{4-12}$$

(i.e., K_z from Eq. (4-10) is evaluated at $z/h = 0.1$)

For local and z-less scaling, define local u_* and $\overline{w\theta}$ from:

$$u_* = u_{*o}(1 - z/h)^{3/4} \tag{4-13}$$

$$\overline{w\theta} = \overline{w\theta}_o (1 - z/h) \tag{4-14}$$

Then in the local scaling layer ($0.1 < z/h$, $h/L > 1$, $z/\Lambda < 1$)

$$K_z = 0.4u_* z/\phi_h(z/\Lambda) \tag{4-15}$$

and in the z-less scaling layer

($0.1 < z/h$, $h/L > 1$, $1 < z/\Lambda < (h/\Lambda) - 10$)

$$K_z = 0.4u_* \Lambda \tag{4-16}$$

Intermittency layer and layer above h ($z/\Lambda > (h/\Lambda) - 10$)

K_z = 0.1 * (K_z at top of near-neutral upper layer (eq. 4-12) or z-less scaling layer (eq. 4-16)).

These equations are consistent with information in the articles by Holtslag and Nieuwstadt (1986), Wyngaard (1985, 1988), Businger (1982), and Tennekes (1982). However, these references seldom discuss the layer above the mixed layer ($z/h > 1$), where we suggest that a small constant value of order 1 m^2/sec be assumed. At these elevations above the mixed layer it may also be necessary to account for wind velocity and temperature gradients in the definition of a local K_z (Hanna 1982):

$$K_z = 0.16(\partial U/\partial z)\ell^2/(1 + 4.5Ri) \qquad (4\text{-}17)$$

where ℓ is the distance to the nearest inversion boundary; however, these values are generally small and are not compatible with the coarse gridding usually chosen for the upper portions of the grid.

The K_z's discussed above are valid only for sub-grid scale dispersion. If the grid size is greater than ℓ, K_z accounts for nearly all of the vertical dispersion. The vertical level spacing algorithm given by Eqs. (3-18) thru (3-20) positions one face at the inversion boundary and helps to ensure that the various sublayers are adequately covered by discrete grid cells.

Computation of the vertical exchange terms, including those due to the spatial and temporal variability of vertical level surfaces is accomplished in the UAM through a fully implicit finite difference scheme. We now use a time-step adaptive algorithm that can choose between Crank-Nicolson (C-N) and fully implicit techniques based on the rapidity of the mixing. The reason for this choice is that the C-N procedure is considerably more accurate at night when diffusivities are small. In addition, we consider all finite vertical flux terms and treat inter-level fluxes such that mass conservation is fully assured.

Section 5

Dry Deposition

Dry deposition is an important removal process for several of the pollutants treated by the CALGRID model. Sehmel (1980) and Hicks (1982) have summarized the factors known to influence dry deposition rates. The most important factors include the characteristics of the surface (e.g., the roughness and composition of the surface, and the type, amount, and physiological state of the vegetation), atmospheric variables (e.g.,stability, turbulence intensity), and the properties of the pollutant (e.g., diffusivity, solubility, and reactivity).

A common measure of deposition is the deposition velocity, defined as:

$$v_d = F/C_s \qquad (5\text{-}1)$$

where, v_d is the deposition velocity (m/s),
F is the pollutant deposition flux ($g/m^2/s$), and,
C_s is the pollutant concentration (g/m^3).

Due to the number and variability of the factors influencing dry deposition rates, reported deposition velocities exhibit considerable variability. For example, SO_2 deposition velocity measurements summarized by Sehmel (1980) range over two orders of magnitude (Figure 5-1). Particle deposition velocities (Slinn et al., 1978) show an even greater variability (Figure 5-2). Although it is not possible to include the effects of all of the factors influencing deposition rates in the deposition model, it is possible, based on the atmospheric, surface, and pollutant properties, to parameterize many of the most important effects.

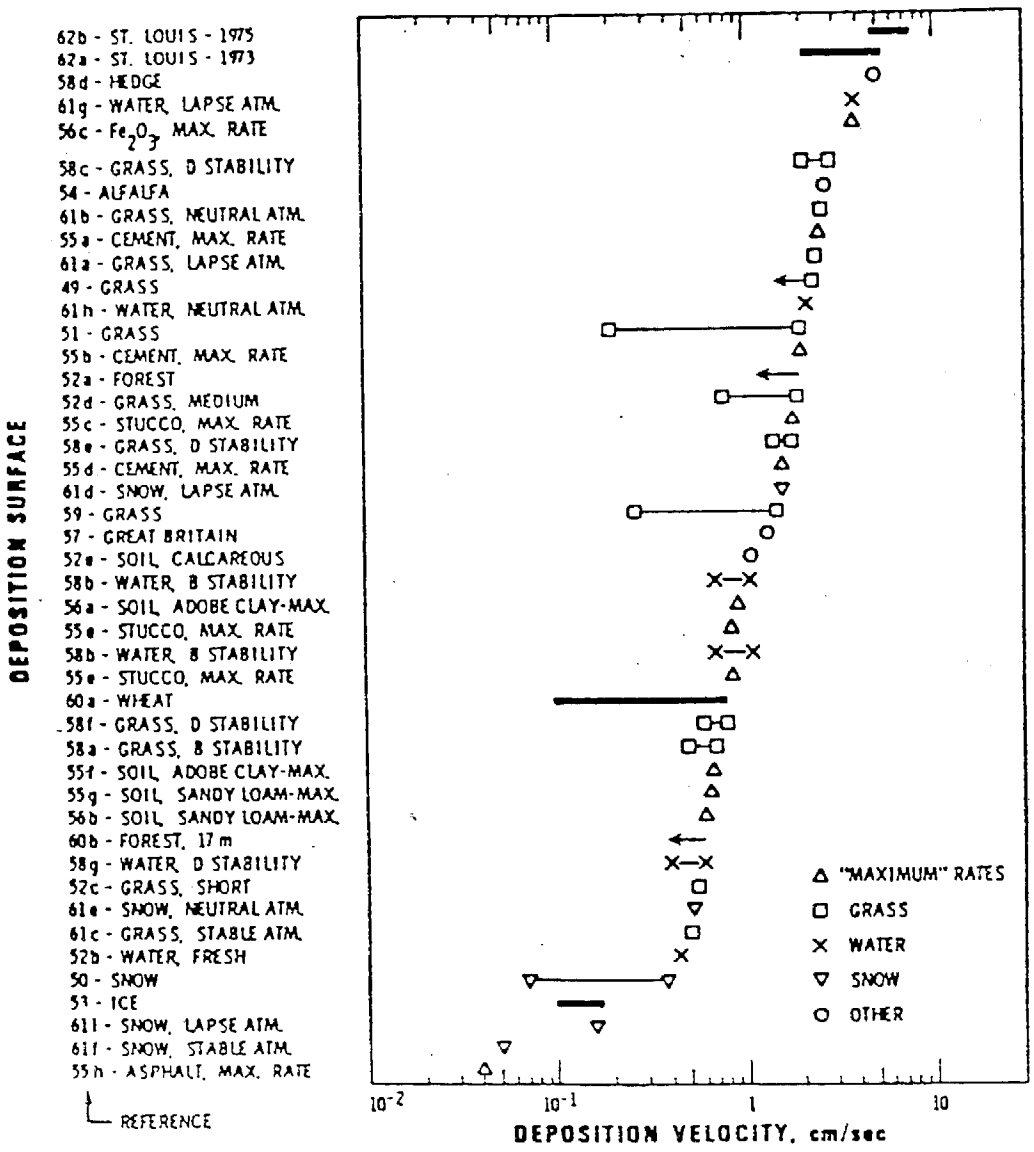

Figure 5-1. Summary of observed SO_2 deposition velocities. [From Sehmel (1980)].

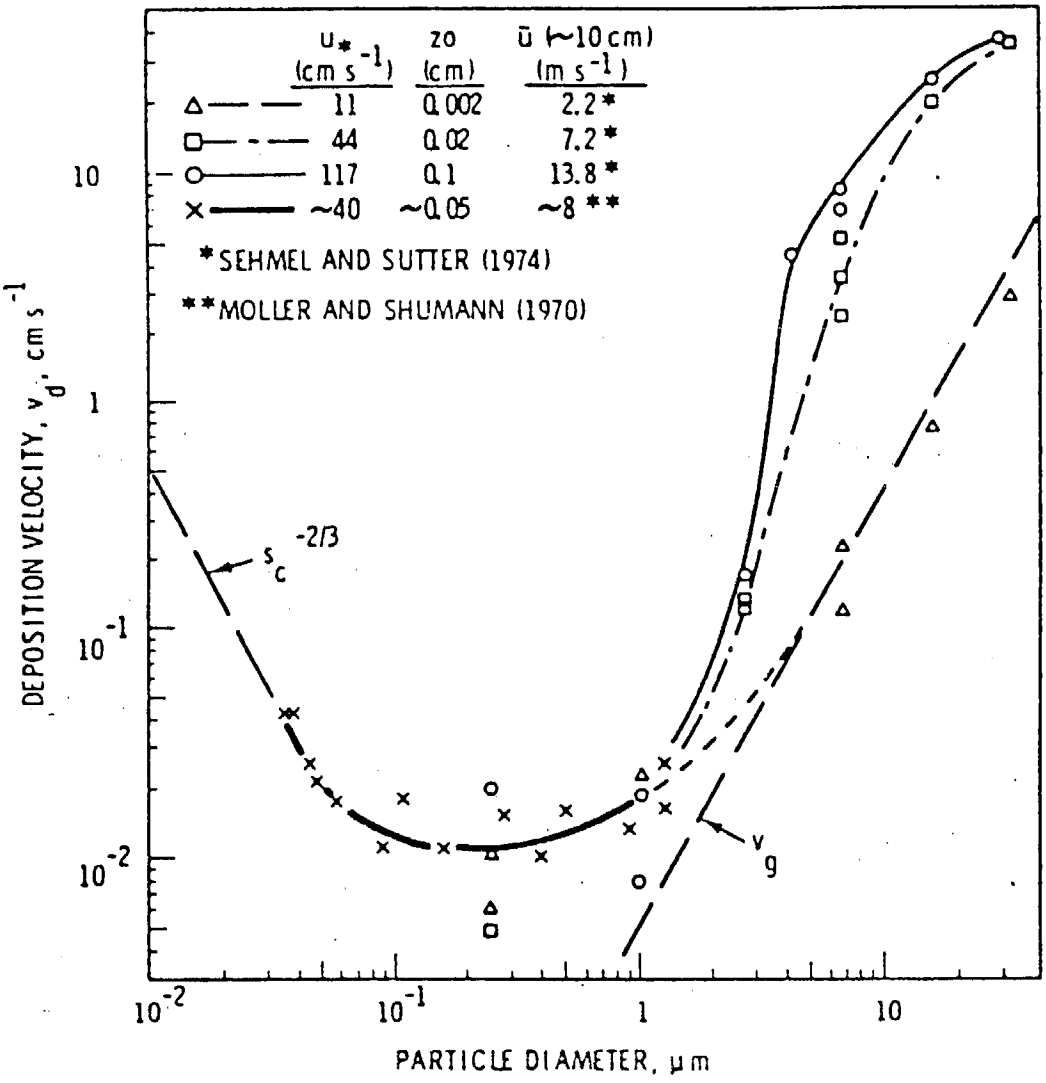

Figure 5-2. Observed deposition velocities as a function of particle size for 1.5 g/cm^3 density particles. Measured by Sehmel and Sutter (1974) and Moller and Schumann (1970). Figure from Slinn et al. (1978).

A convenient framework for this parameterization is the resistance model. In this approach, the deposition velocity is expressed as the inverse of a sum of "resistances". Each resistance represents the opposition to the movement of the pollutant through the atmosphere to the surface.

In the Eulerian grid framework, pollutant diffusion between model layers is determined by the vertical diffusivities (see Section 4.2). The deposition module needs to consider three sublayers within the lowest CALGRID model layer as illustrated in Figure 5-3.

(1) **Surface Layer.** The surface layer is a shallow layer next to the ground that is within the atmospheric constant flux layer. The top of the surface layer will correspond to the top of the lowest model grid cell, which is approximately 20 m. The atmospheric resistance, r_a, is used to parameterize the rate of pollutant transfer within this sublayer as a function of atmospheric turbulence and stability, and surface characteristics (Wesely and Hicks, 1977; Hosker, 1974).

(2) **Deposition Layer.** The deposition layer is a thin, non-turbulent layer that develops just above the surface. For rough surface, this layer is constantly changing and is likely to be intermittently turbulent (Hicks, 1982). The primary transfer mechanisms across the laminar deposition layer are molecular diffusion for gases and Brownian diffusion and inertial impaction for particles. The deposition layer resistance, r_d, is usually parameterized in terms of the Schmidt number (viscosity of air divided by the diffusivity of the pollutant) and, for particles, the Stokes number (which is a function of the gravitation settling velocity, friction velocity, and the viscosity of air).

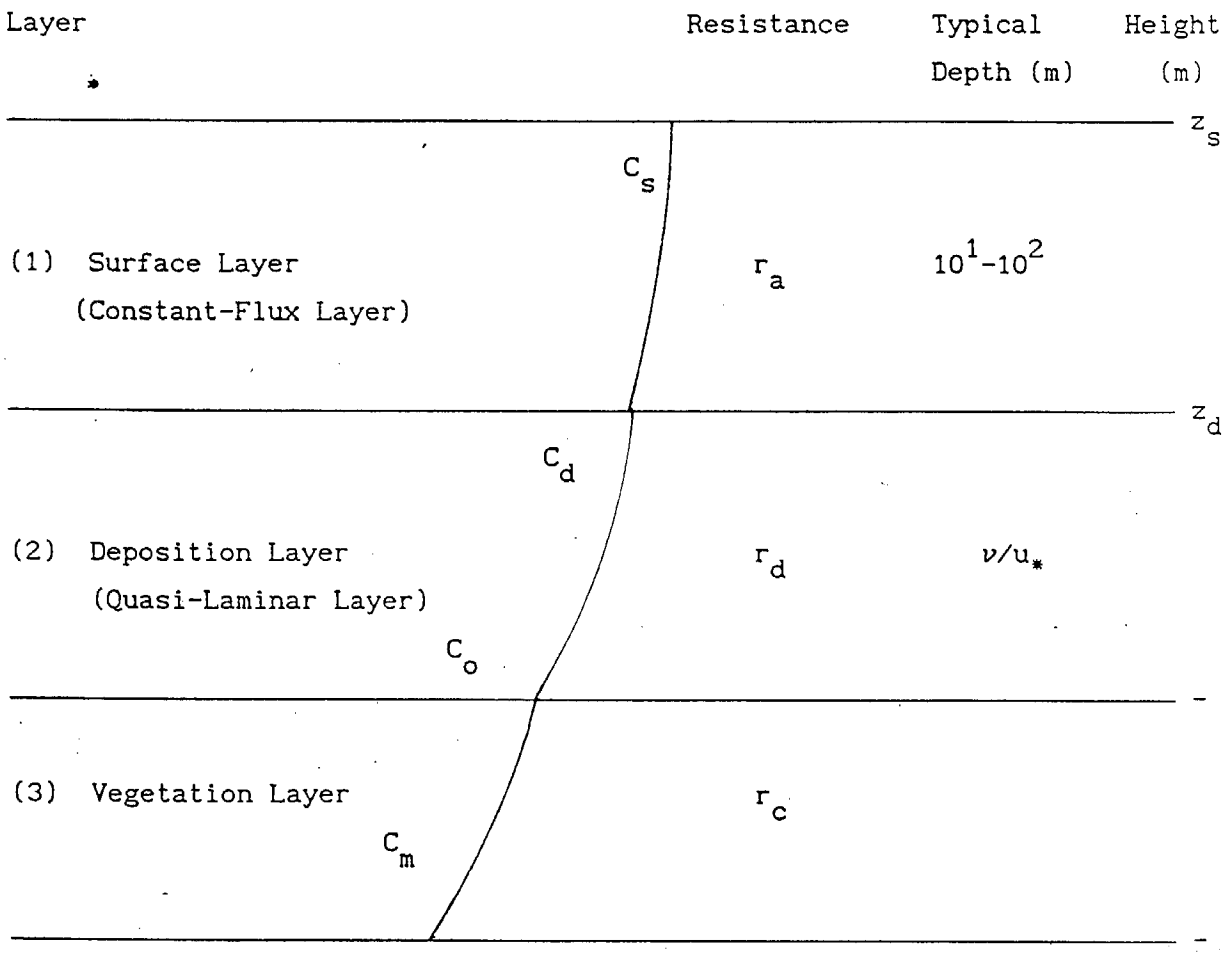

Figure 5-3. Multilayer structure used in the dry deposition resistance model. (Adapted from Slinn et al., 1978).

(3) **Vegetation Layer.** Vegetation is a major sink for many soluble or reactive gaseous pollutants. After passing through the stomata, soluble pollutants dissolve in the moist mesophyll cells in the interior of the leaves. Reactive pollutants, such as O_3, may also interact with the exterior (cuticle) of the leaves. Due to the response of the stomata to external factors such as moisture stress, temperature, and solar radiation, the resistance in the vegetation layer, r_c, can exhibit significant diurnal and seasonal variability. An alternate pathway included in the vegetation layer is deposition directly to the ground or water surface.

Model Options

Three options are provided in the model for different levels of detail in the treatment of dry deposition processes.

- Full treatment of spatially and temporally varying gas/particle deposition rates predicted by a resistance deposition model, as described in Section 5.1 and 5.2.

- User-specified 24-hour cycles of deposition velocities for each pollutant. This option will allow a "typical" time dependence of deposition to be incorporated, but will not include any spatial dependencies.

- No dry deposition.

These options provide increased flexibility and will facilitate sensitivity testing of the model.

5.1 Deposition of Gases

At the reference height, z_s, the deposition velocity for gases can be expressed (Wesely and Hicks, 1977; Hicks, 1982) as the inverse of a sum of resistances in Layers 1 through 3:

$$v_d = (r_a + r_d + r_c)^{-1} \qquad (5\text{-}2)$$

where r_a is the atmospheric resistance (s/m) through the surface layer,
r_d is the deposition layer resistance (s/m), and,
r_c is the canopy (vegetation layer) resistance (s/m).

Atmospheric Resistance

The atmospheric resistance can be obtained by integration of the micrometeorological flux-gradient relationships (Wesely and Hicks, 1977):

$$r_a = \frac{1}{k\, u_*} \left[\ln (z_s/z_o) - \phi_H \right] \qquad (5\text{-}3)$$

where z_s is the reference height (m),
z_o is the surface roughness length (m),
k is the von Karman constant (~0.4),
u_* is the friction velocity (m/s),
ϕ_H is a stability correction term, and,
L is the Monin-Obukhov length (m).

The stability correction term accounts for the effects of buoyancy on the eddy diffusivity of the pollutant. It is assumed that the pollutant transfer is similar to that for heat (Wesely and Hicks, 1977). A gridded field of surface roughness lengths is passed to the model in the output file of the meteorological model, CALMET. The surface roughness length is either estimated from the predominant land use of each grid cell, or, if available, based on actual values entered by the user. Over water, due to the effect of

the wind on wave height, the surface roughness length varies as a function of wind speed. Hosker (1974) parameterizes z_o over water as:

$$z_o = 2.0 \times 10^{-6} u^{2.5} \quad (5\text{-}4)$$

where u is the wind speed (m/s) at 10 m.

Because the concentration in the lowest layer is a vertical average through the cell depth, Eq. (5-3) must be vertically integrated in order to provide the proper cell resistance. Pleim et al. (1984) found that a good approximation of the integrated expression can be obtained by substituting z_s in Eq. (5-3) with

$$z = \frac{\Delta z - z_1}{e} + z_1 \quad (5\text{-}5)$$

$$\Delta z = z_2 - z_1 \quad (5\text{-}6)$$

where Δz is the depth (m) of the lowest grid cell,

z_1, z_2 are the bottom and top face heights (m) of the first grid cell, and,

e is the base of natural logarithms (2.7182818).

Deposition Layer Resistance

Due to the importance of molecular diffusion to the transport through the laminar deposition layer, the deposition layer resistance for gaseous pollutants is parameterized in terms of the Schmidt number:

$$r_d = d_1 Sc^{d_2}/(k u_*) \quad (5\text{-}7)$$

where S_c is the Schmidt number (ν/D),

ν is the kinematic viscosity of air (m^2/s),

D is the molecular diffusivity of the pollutant (m^2/s), and,

d_1, d_2 are empirical parameters.

Experimental studies summarized by Hicks (1982) suggest a range of values for the empirical variables of 1.6 to 16.7 for d_1 and 0.4 to 0.8 for d_2. Intermediate values of $d_1 = 5$, and $d_2 = 2/3$ are recommended based on Shepherd (1974), Slinn et al. (1978), and Hicks (1982).

Canopy Resistance

The canopy resistance is the resistance for gases in the vegetation layer. There are three main pathways for uptake/reaction of the pollutant within the vegetation or surface:

(1) Transfer through the stomatal pore and dissolution or reaction in the mesophyll cells.

(2) Reaction with or transfer through the leaf cuticle.

(3) Transfer into the ground/water surface.

In the resistance model, these pathways are treated as three resistances in parallel.

$$r_C = [LAI/r_f + LAI/r_{cut} + 1/r_g]^{-1} \quad (5\text{-}8)$$

where r_f is the internal foliage resistance (s/m) (Pathway 1),
r_{cut} is the cuticle resistance (s/m), (Pathway 2),
r_g is the ground or water surface resistance (s/m), (Pathway 3), and,
LAI is the leaf area index (ratio of leaf surface area divided by ground surface area). The LAI is specified in the model as a function of land use type.

The first pathway is usually the most important for uptake of soluble pollutants in vegetated areas. As illustrated schematically in Figure 5-4, r_f consists of two components:

$$r_f = r_s + r_m \quad (5\text{-}9)$$

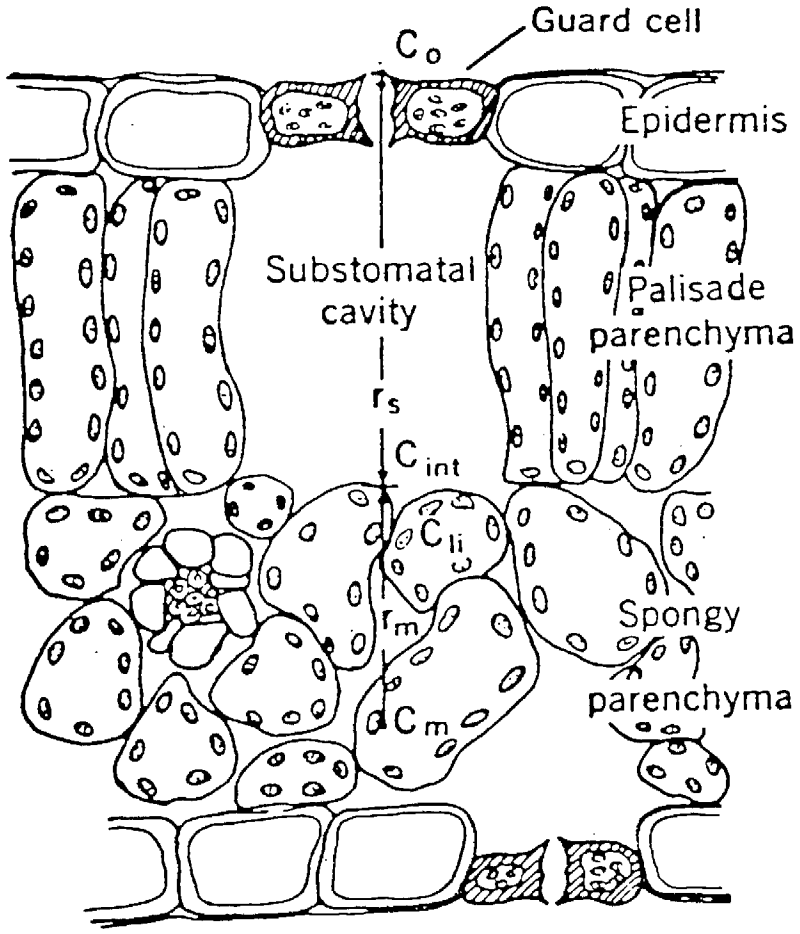

Figure 5-4. Schematic cross-section of a leaf illustrating the internal foliage resistance to pollutant transfer through the stomatal pore, substomatal cavity, and into the mesophyll (spongy parenchyma) cells. [From O'Dell et al., (1977)].

where r_s is the resistance (s/m) to transport through the stomatal pore, and
r_m is the resistance (s/m) to dissolution or reaction of the pollutant in the mesophyll (spongy parenchyma) cells.

Stomatal action imposes a strong diurnal cycle on the stomatal resistance, and, due to its important role for gaseous, soluble pollutants such as SO_2, on the deposition velocity. Stomatal opening/closing is a response to the plant's competing needs for uptake of CO_2 and prevention of water loss from the leaves. The stomatal resistance can be written (O'Dell et al., 1977) as:

$$r_s = p/(bD) \qquad (5\text{-}10)$$

where p is a stomatal constant ($\approx 2.3 \times 10^{-8}$ m^2),
b is the width of the stomatal opening (m), and,
D is the molecular diffusivity of the pollutant (m^2/s).

The width of the stomatal opening is a function of the radiation intensity, moisture availability, and temperature. The variation of b during periods when vegetation is active can be represented (Pleim et al., 1984) as:

$$b = b_{max} [S/S_{max}] + b_{min} \qquad (5\text{-}11)$$

where b_{max} is the maximum width (m) of the stomatal opening ($\sim 10 \times 10^{-6}$ m),
b_{min} is the minimum width (m) of the stomatal opening ($\sim 0.1 \times 10^{-6}$ m),
S is the solar radiation (W/m^2) received at the ground, and
S_{max} is the solar radiation (W/m^2) at which full opening of the stomata occur.

However, during periods of moisture stress, the need to prevent moisture loss becomes critical, and the stomata close. It can be assumed that $b = b_{min}$ for unirrigated vegetation under moisture stress conditions. When vegetation is inactive (e.g., during the seasonal dry periods in much of California), the internal foliage resistance becomes very large, essentially cutting off Pathway 1. In CALGRID, the state of the unirrigated vegetation is specified

as one of these states (A) active and unstressed, (B) active and stressed, or (C) inactive.

The effect of temperature on stomatal activity has been reviewed by Pleim et al. (1984). The most significant effects are due to temperature extremes. During cold periods ($T < 10\ ^{\circ}C$), metabolic activity slows, and b is set equal to b_{min}. During hot weather conditions ($T > \sim 35\ ^{\circ}C$), the stomata are fully open ($b = b_{max}$) to allow evaporative cooling of the plant (assuming the vegetation is in state A - active and unstressed). These temperature effects provide additional bounds on the value of r_f given by Eq. (5-9).

Mesophyll Resistance

The mesophyll resistance depends on the solubility and reactivity of the pollutant. It is an input parameter supplied to the deposition model for each gaseous species. O'Dell et al. (1977) estimate the mesophyll resistance for several pollutants. For soluble pollutants such as HF, SO_2, Cl_2 and NH_3, $r_m \sim 0.0$. The mesophyll resistance can be large for less soluble pollutants such as NO_2 (~500 s/cm) and NO (9400 s/cm). For other pollutants, r_m can be estimated based on the solubility and reactivity characteristics of the pollutant.

Cuticle Resistance

The second pathway for deposition of gases in the vegetation layer is via the leaf cuticle. This includes potential direct passage through the cuticle or reaction of the pollutant on the cuticle surface. Hicks (1982) notes that measurements of SO_2 deposition to wheat (Fowler and Unsworth, 1979) show significant cuticle deposition. However, Hosker and Lindberg (1982) suggest that passage of gases through the cuticle is negligible. Therefore, the cuticle deposition is likely to be controlled by the pollutant reactivity. Pleim et al. (1984) parameterize r_{cut} as a function of the pollutant reactivity of the depositing gas relative to the reference values for SO_2.

$$r_{cut} = (A_{SO_2}/A)\ r_{cut}(SO_2) \qquad (5\text{-}12)$$

where A is the reactivity parameter for the depositing gas,

A_{SO_2} is the reactivity of SO_2 (~8.0), and,

$r_{cut}(SO_2)$ is the empirically determined cuticle resistance (s/m) of SO_2.

Pleim et al. (1984) suggest $r_{cut}(SO_2)$ is about 17 s/cm. Reactivity values for other pollutants are estimated at 8.0 (NO_2), 15.0 (O_3), 18.0 (HNO_3), and 4.0 (PAN).

Ground/Water Resistance

The third pathway through the "vegetation layer" does not involve vegetation at all. It is deposition directly to the ground or water surface. In moderately or heavily vegetated areas, the internal foliage and cuticle resistances usually control the total canopy resistance. However, in sparsely vegetated area of California, deposition directly to the surface may be an important pathway. Over water, deposition of soluble pollutants can be quite rapid.

The ground resistance, r_g, over land surfaces can be expressed (Pleim et al., 1984) relative to a reference value for SO_2:

$$r_g = (A_{SO_2}/A)\ r_g(SO_2) \qquad (5\text{-}13)$$

where $r_g(SO_2)$ is the ground resistance of SO_2 (~5 s/cm).

Slinn et al. (1978) parameterize the liquid phase resistance of the depositing pollutant as a function of its solubility and reactivity characteristics. Their results can be expressed as:

$$r_g = H/(\alpha_* d_3 u_*) \qquad (5\text{-}14)$$

where H is the Henry's law constant (ratio of gas to liquid phase concentration of the pollutant),

α_* is a solubility enhancement factor due to the aqueous phase reactivity of the pollutant ($\alpha_* \sim 10^3$ for SO_2, ~1 for CO_2), and,

d_3 is a constant (-4.8×10^{-4}).

5.2 Deposition of Particulate Matter

In the CALGRID model, H_2SO_4 is treated as particulate sulfate for purposes of computing its rate of dry removal. Because particulate matter does not interact with vegetation in the same way as gaseous pollutants, particle deposition velocities are commonly expressed only in terms of r_a, r_d and a gravitational settling term. The resistance in the vegetation layer (r_c) is not a factor because once penetrating the deposition layer, particles are usually assumed to stick to the surface (e.g., Voldner et al., 1986). Therefore, their behavior is similar to highly soluble/reactive gases with $r_c \sim 0$. Based on an assumption of steady-state conditions, the deposition velocity for particles can be expressed (Slinn and Slinn, 1980; Pleim et al., 1984) as:

$$v_d = (r_a + r_d + r_a r_d v_g)^{-1} + v_g \qquad (5\text{-}15)$$

where v_g is the gravitational settling speed (m/s) of the particle.

The atmospheric resistance, r_a, is obtained from Eq. (5-3). There are three major mechanisms for transport of particles across the deposition layer. Small particles (< 0.1 μm diameter) are transported through the laminar deposition layer primarily by Brownian diffusion. This process becomes less efficient as the particle diameter increases. Particles in the 2-20 μm diameter range tend to penetrate the deposition layer by inertial impaction. The stopping time, t, defined as the settling velocity divided by the acceleration due to gravity, is a measure of tendency of a particle to impact. Inertial impaction is most effective in the 2-20 μm diameter range. Larger particles are dominated by gravitational settling effects. The effect of the terms involving v_g in Eq. (5-15) always is to increase the deposition

velocity. Particles in the range of 0.1-2 μm diameter range, such as sulfate, have very small settling velocities and are not efficiently transported across the deposition layer by either the Brownian diffusion or the inertial impaction mechanism. As a result, these particles have the lowest deposition velocities (see Figure 5-2).

The deposition layer resistance can be parameterized (e.g., Pleim et al. 1984) in terms of the Schmidt number ($Sc = \nu/D$, where ν is the viscosity of air, and, for particles, D is the Brownian diffusivity of the pollutant in air) and the Stokes number ($St = (v_g/g)(u_*^2/\nu)$, where v_g is the gravitational settling velocity and g is the acceleration due to gravity).

$$r_d = (Sc^{-2/3} + 10^{-3/St})^{-1} u_*^{-1} \qquad (5\text{-}16)$$

The diffusivity of a particle in air, D, is a function of the particle size. Smaller particles tend to be more efficiently transported by Brownian motion, and therefore have higher diffusivities. The Stokes number is a measure of the likelihood of impaction of the particle. It increases with increasing particle size.

The gravitational settling velocity is a function of the particle size, shape, and density. For spheres, the settling velocity is given by the Stokes equation:

$$v_g = [(d_p)^2 g (\rho_p - \rho_g) C]/(18 \nu) \qquad (5\text{-}17)$$

where d_p is the particle diameter (m)
ρ_p is the particle density (g/m^3),
ρ_g is the air density (g/m^3), and,
C is the Cunningham correction for small particles. This correction given by:

$$C = 1 + (2 \lambda / d_p)[a_1 + a_2 \exp(-a_3 d_p/\lambda)] \qquad (5\text{-}18)$$

where λ is the mean free path of air molecules (6.53×10^{-6} cm), and
a_1, a_2, a_3 are constants (1.257, 0.40, 0.55, respectively).

Because of the sensitivity of the deposition velocity to particle size, the effective deposition velocity is computed for a number of individual size categories, and then weighted by the actual size distribution. For sulfate, the geometric mass mean diameter is approximately 0.5 μm with a geometric standard deviation of approximately 2 μm.

Section 6

Integration of the Chemical Kinetics Equations

6.1 Introduction:

The treatment of the chemical portion of comprehensive air pollution models requires special attention. This is due to the fact that up to 90% of the computation time in urban airshed and regional-scale photochemical oxidant simulations is spent solving the equations describing the chemistry. Typically, photochemical oxidant models include 20-100 chemical species involved in one-to-several hundred chemical reactions. The equations resulting from these chemical mechanisms are stiff, highly coupled, and nonlinear. Thus, the simulation time of oxidant models is determined to a large degree by the computational burden associated with the solution of the chemistry equations.

In addition to the computation burden of a given chemical mechanism used in oxidant models, the other major concern in the formulation of such models is the need to provide flexibility in the code so that chemical mechanisms can be changed readily. Our understanding of the photochemistry of the polluted troposphere continues to improve and thus, the photochemical mechanisms are continuously evolving. It is therefore desirable to formulate an oxidant model in such a way that the chemical mechanism can be easily modified or replaced with an alternative mechanism. The chemical formulation and integration scheme incorporated in the CALGRID model is fast and accurate and is easily modified to accept alternative mechanisms. The details are described in the following sub-sections and in the User's Guide.

6.2 Numerical Integration of the Chemistry Equations

The inclusion of chemical reactions into airshed models necessitates the solution of sets of coupled, non-linear, and stiff ordinary differential equations (i.e., O.D.E.'s). ODE's are stiff when the eigenvalues of the Jacobian matrix vary over many orders of magnitude. This problem was first

pointed out as important in practical numerical problems by Curtiss and Hirschfelder (1952). Dahlquist (1963) pointed out that the resulting instability is the cause of the difficulty. Thereafter, a large literature on the numerical solution of stiff systems developed.

There have been several survey studies conducted assessing the efficiency of the various ODE solvers and reviewing the difficulty of solving stiff problems. The first review was by Seinfeld, Lapidus, and Hwang (1970); this was followed chronologically by Bjurel et al. (1970), Gelinas (1972), Willoughly (1974), Enright (1975), Lapidus and Schiesser (1976), and Warner (1977). However, since the time of these studies additional developments and improvements in numerical methods for O.D.E.'s have occurred. An updated survey study reflecting more current integration techniques was done recently (Shieh et al., 1988).

The inclusion of photochemistry into the grid models presents a severe numerical challenge because the resulting system of equations contains eigenvalues ranging over ~ 15 orders of magnitude. The choice of the method used depends not only on the nature of the application but also on the imposed constraints (e.g., computation time, accuracy, difficulty of implementation, vectorization, etc.).

The implicit techniques such as Gear's methods have become standard techniques. However, Gear's methods are very expensive since they require the inversion of large matrices or the solution of large sets of nonlinear equations. Furthermore, Gear's methods can also generate negative concentrations. In recent years, investigators are utilizing quasi-steady techniques based on the work of Hesstvedt et al. (1970) and McRae et al. (1982). These techniques are faster than Gear's method by 5 to 100 times, generate only non-negative concentrations, and are more readily vectorizable.

The present AIRSHED model utilizes a Crank-Nicolson integration scheme, whereas the CALTECH model uses the hybrid solver developed by McRae et al. (1982). In the CALGRID model, the user can select either the hybrid solver or the Quasi Steady State Analysis (i.e., QSSA) method. Both of these methods represent techniques which make use of asymptopic or "quasi-linear"

assumptions. These techniques write the chemistry equations to be integrated in the form

$$\frac{dC_i}{dt} = P_i(\underline{C}) - D_i(\underline{C})\, C_i \qquad (6\text{-}1)$$

$$i = 1\ldots,N_{All}$$

where C_i is the concentration of the ith species, P_i and D_i are the production and loss terms for the ith species, respectively, i and j are species indices, and N_{All} is the total number of non-constant species included in the chemical analysis.

The hybrid solver used by McRae et al. (1982) is based on the second-order predictor, interated corrector scheme developed by Young and Boris (1977). The stiff equations are solved according to predictor:

$$C^*_{i,n} = \frac{C_{i,n-1}\,[2\tau_{i,n-1} - \delta t] + 2\delta t\, \tau_{i,n-1}\, P_{i,n-1}}{2\,\tau_{i,n-1} + \delta t} \qquad (6\text{-}2)$$

and corrector:

$$C^m_{i,n} = Q\,[\tau^{m-1}_i + \tau_{i,n-1}]\,[P^{m-1}_i + P_{i,n-1}] + C_{i,n-1}\,[\tau^{m-1}_i + \tau_{i,n-1} - \delta t] \qquad (6\text{-}3)$$

where $$Q = \frac{\delta t}{2\,(\tau^{m-1}_i + \tau_{i,n} + \delta t)}$$

In these equations, the subscripts n and n-1 denote the time levels and the superscripts m and m-1 indicate the corrector step iteration number. In addition, $\tau_{i,n-1} = 1/D_{i,n-1}$ is used in the predictor step and $\tau_i^{m-1} = 1/D_i^{m-1}$, is used in the corrector step. The time step to advance from the n-1 th time level to the nth level is selected according to the relation

$$\delta t = \epsilon_i \min \left\{ \frac{C_{i,n-1}}{P_{i,n-1} - D_{i,n-1} C_{i,n-1}} \right\} \qquad (6\text{-}4)$$

The QSSA technique was developed by Hesstvedt, Hov and Isaksen (1978). If the production (i.e., P_i) and the destruction terms (D_i) are assumed constant over the time step δt, then this equation can be solved analytically, i.e.,

$$C_n = \frac{P_i}{D_i}(1 - e^{D_i \delta t}) + C_{n-1} e^{-D_i \delta t} \qquad (6\text{-}5)$$

The accuracy of this method is dependent on the careful choice of δt. Hesstvedt et al. (1978) presented a scheme by which Eq (6-5) is used only for species where $\delta t/10 \leq \tau_i \leq 100\ \delta t$. For species where $\tau_i \gg \delta t$ a simple explicit Euler's integration is recommended, and for species where $\tau_i < \delta t/10$ values are calculated based on the assumption of local equilibrium, i.e., $C_N = \frac{P_n}{D_n}$.

The hybrid solver has been tested extensively by McRae et al. (1982) using the chemical mechanism originally built into the airshed model and has been compared to results obtained by the use of EPISODE (one of Gear's methods). Samples results are presented in Table 6-1.

Table 6-1. Comparison of the start-up times for EPISODE and hybrid solution scheme for typical smog chamber experiment (from McRae et al. 1982).

Time (min)	Species	Concentration (parts-per-million by volume) Episode	Hybrid solver	Computer time (ms) per 30 minute step Episode	Hybrid
30	NO	0.0567	0.0567 (0.00)*	1014	152
	NO_2	0.4070	0.4077 (0.17)		
	O_3	0.0834	0.0832 (−0.24)		
60	NO	0.0202	0.0203 (0.50)	175	104
	NO_2	0.3889	0.3914 (0.64)		
	O_3	0.2191	0.2194 (0.14)		
90	NO	0.0110	0.0107 (−2.73)	79	81
	NO_2	0.3329	0.3290 (−1.17)		
	O_3	0.3383	0.3450 (1.98)		
120	NO	0.0066	0.0062 (−6.06)	47	70
	NO_2	0.2652	0.2557 (−3.58)		
	O_3	0.4391	0.4497 (2.41)		
				1315 ms	407 ms

* Percentage difference between EPISODE and Hybrid solution technique = 100 [Hybrid/EPISODE − 1].

For comparison purposes the QSSA method, as implemented in the STEM-II model (cf, Carmichael, et al. (1986)), is compared with results obtained using the Gear's method. To better understand the trade-offs between the asymptotic methods and Gear's method, a multiday box model calculation using the Lurman, Lloyd, Atkinson (1986) chemical mechanism (referred to as LLA) was performed. The LLA mechanism consists of 53 chemical species and 112 chemical reactions. The QSSA method is as indicated by Eq.(6-5). However, the time steps are fixed at 30 seconds during the daytime, 60 seconds at nighttime and 12 seconds at sunrise and sunset. (These are the present time steps fixed in the QSSA method and included in the CALGRID model).

The comparisons between Gear's method and the QSSA method are performed for the simulation of gas phase kinetics in a box model. In order to emphasize only the chemistry, the physical processes such as emissions, depositions, dilutions, transports, etc. are not included. The test simulation adopted initial concentrations typical of polluted areas near sunrise: 40 ppb of NO, 10 ppb of NO_2, 20 ppb of SO_2, 1 ppb of O_3, 30 ppb of alkanes, 8 ppb of ethene, 7 ppb of alkenes, 10 ppb of aromatics, 7 ppb of aldehydes and 1 ppb of ketones. Typical background concentrations for CH_4 and CO of 1650 and 125 ppb, respectively, were also included throughout this simulation. The ambient temperature and relative humidity were held to be fixed at 20 °C and 50%, respectively. A multi-day simulation for the summer solstice at 40 N latitude was employed. The comparisons for key species are shown in Figure 6-1. The percentage relative error based on results from the Gear's method show that SO_2, sulfate, O_3, NO and NO_2 are less than 1% after 2 days of simulation.

Another important concern in the chemical integration is whether the method conserves mass. Figure 6-2 shows the percent relative error in the mass balance of sulfur and nitrogen for the test problem. As shown, the use of the QSSA method often fails to maintain the mass balance. Moreover, the strong coupling between more reactive species results in numerical instability if a relatively long time step is used. Implementation of a linear transformation (or lumping) technique allows the circumvention of these two main difficulties. These procedures are explained in detail in Hesstvedt et al. (1978).

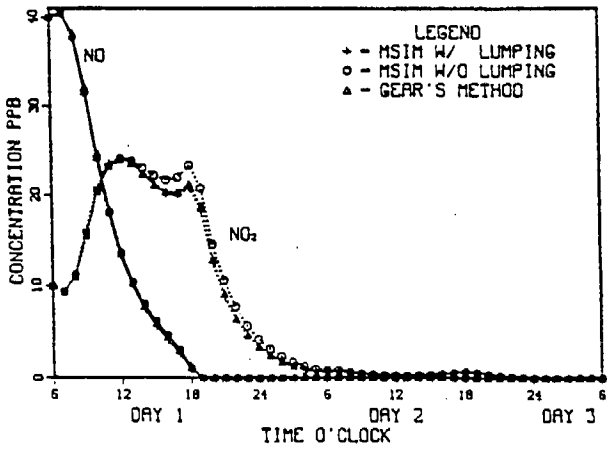

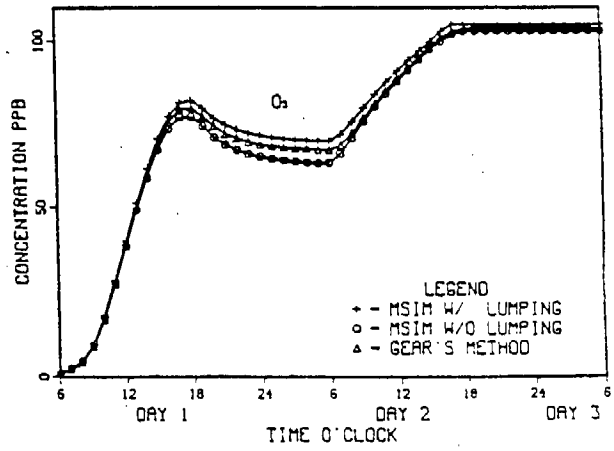

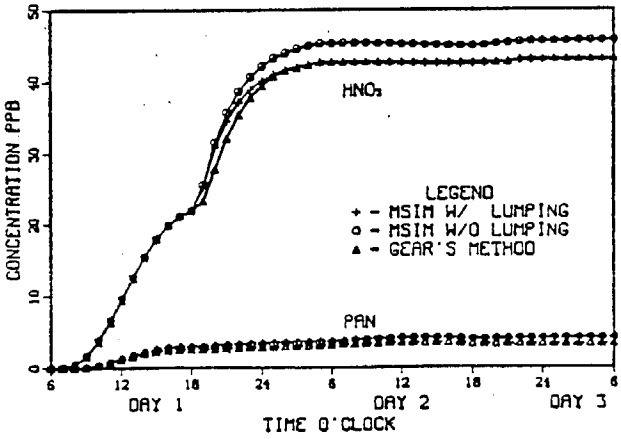

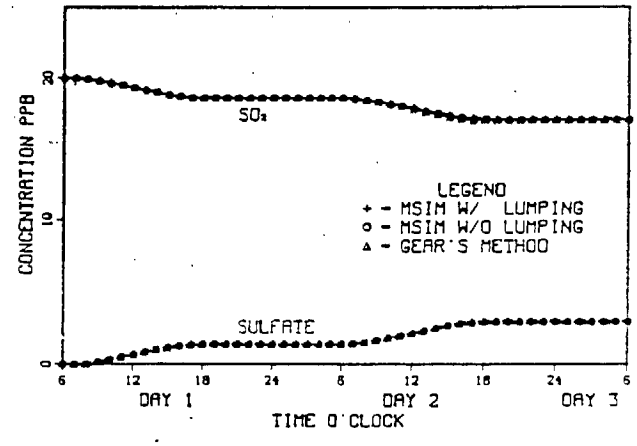

Figure 6-1. Comparison between the QSSA method GEAR's method.

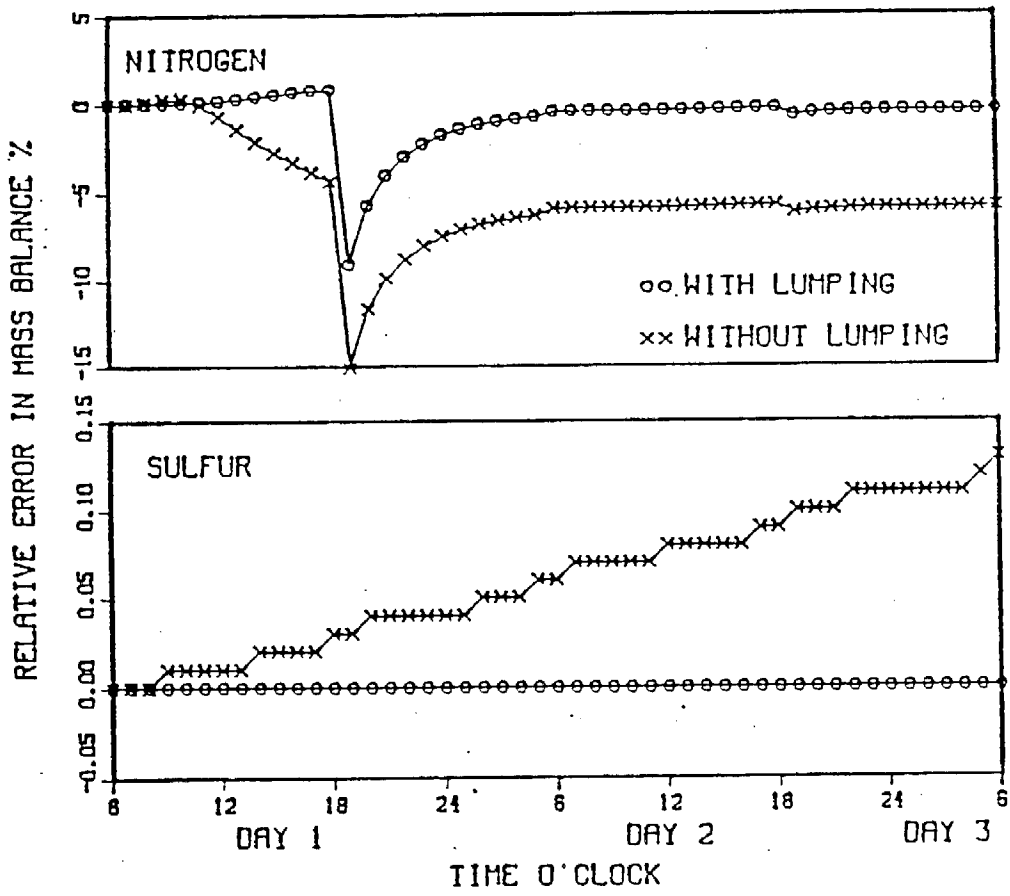

Figure 6-2. Comparison of the mass balance--with and without lumping.

Results using the QSSA method with lumping are presented in Figures 6-1 and 6-2. Clearly, the lumping technique maintains the mass exactly for sulfur and within 0.5% for nitrogen throughout the simulation, except at the peak occurring around 18:00 of the first day. This seems to arise from numerical stiffness associated with the dramatic change in chemistry which occurs at sunset. The QSSA method executes ~ 10 times faster than Gear's method for this application. The lumping procedure is included in the QSSA method incorporated in the CALGRID model.

Comparisons of the hybrid and QSSA methods as implemented in the CALGRID are presented in section 6-4.

Even with fast chemical integration techniques, such as those described above, the cost of solving the chemistry remains high. One procedure commonly used to decrease the computation time further is to reduce the stiffness of the chemical equations by employing the pseudo steady-state approximation. The basic idea behind the pseudo steady-state approximation is that the very short-lived species can be approximated by their equilibrium values. The use of this assumption leads to a reduction in computation time by:

1) reducing the number of chemical species, N_{trans} which are treated as transported species in the model (Each transported species is described by the atmospheric diffusion equation, and thus requires the solution of Eq. 6-1); and

2) reducing the stiffness of the remaining system of equations, and thus allowing a larger time step to be used in the integration.

When the pseudo steady-state approximation is used, Eq. 6-1 is replaced by:

$$\frac{dC_i}{dt} = P_i(C_j) - D(C_j)\, C_i \qquad i = 1,\ldots N_{trans} \qquad (6\text{-}6)$$

$$j = 1,\ldots N_{All}$$

$$R_k (C_j) = 0, \; k = 1, \ldots, N_{ss} \qquad (6\text{-}7)$$

where N_{trans} is the number of species not treated as steady-state, N_{ss} is the number of species treated as steady-state species, and $N_{trans} = N_{all} - N_{ss}$. Note that the species treated by the pseudo steady-state approximation are determined by solution of the nonlinear algebraic equations (6-7) and do not require numerical integration.

The main difficulty associated with the use of the pseudo steady-state approximation is the a priori choice of which species can be treated by this assumption. There is no well-developed theory to guide this choice. Approximate methods are often used which are based on eigenvalue-eigenvector analysis (McRae et al., 1982). In the development of the CALGRID mechanism, the choice of which species to analyze as transported and which to analyze as pseudo steady-state species is treated as an input condition.

6.3 Inclusion of Chemical Mechanism into the CALGRID Model

The CALGRID model has been structured so that the chemical mechanism can be modified or exchanged easily and without the need to perform extensive recoding. To facilitate the ease of modifying the chemical mechanism, the procedures developed by Carter (1988) are incorporated into the model. The primary feature of this treatment is that the chemical mechanism is read as an input file (LMPBE221,MOD) to CALGRID. This file contains the details of the chemical mechanism, such as; the species included, the specific reactions, the rate constants, photolysis data, and the hydrocarbon lumping. This file, fully described in the User's Guide, also contains the number and names of species which are to be treated as transported species or pseudo steady-state species. Carter's mechanism software also produces the mechanism specific subroutines names CONSTR, DIFUN and BLDUP which are used in the CALGRID model to formulate the equations used in the chemical integration (i.e., Eqs. (6-6) and (6-7)). Thus, to change the chemical mechanism, one need only change the input files and the three mechanism specific subroutines. (Carter (1988) also has prepared software to easily generate the input files.

The current model also makes use of Carter's scheme for the preparation of the emissions data, so that the emissions are consistent with the chemical mechanism selected (i.e., classifying the hydrocarbon emissions according to the lumping scheme used), and adjusts emissions specific parameters of the chemical mechanism. These procedures are also described in Carter (1988).

The chemical integration procedures have been tested using the Carter chemical mechanism identified as LMPBE221.MOD. A complete listing of the input file associated with this mechanism is presented in the User's Guide. This mechanism is described in detail by Carter (1988) and is quite similar to the LLA mechanism (1986). This mechanism contains 50 chemical species and 102 chemical reactions. It uses 4 alkanes and 2 alkenes in the lumping of the hydrocarbons; two concentrations (O_2, m) are treated as constants, and ten species (OH, O, O('D), RO_2-R^0, RO_2-N^0, $R_2O_2^0$, RO_2-XN, $HOCOO^0$, NO_2^0, and O_3OL-5B^0) are treated under the pseudo steady-state approximation. Also, a unit photon concentration, $h\nu$, is held fixed as a parameter, whereas the H_2O concentration is updated on an hourly and cell-by-cell basis. The actual mechanism is listed (as lines 197-333 of LMPBE221.MOD) in Table 6-2.

Within the treatment of the chemical mechanism, the thermal reactions are specified using an extended Arrhenius kinetics expression, i.e.,

$$k = A * (TEMP/TREF)**B*exp[-E_a/0.0019877*TEMP] \qquad (6\text{-}8)$$

where TEMP is the ambient temperature in K, A is the Arrhenius pre-exponential factor, Ea is the activative energy in kcal/mol, and B is a unitless quantity. Thermal reactions which are not at their high pressure limit, are treated using the Troc falloff expression (see Carter (1988)).

The rate constants for the photolysis reactions are calculated using the intensity and spectral distribution of the light source, and the absorption coefficients and quantum yields of the photolysis reactions, i.e.,

Table 6-2

Listing of the chemical reactions involved in the LMPBE221 chemical mechanism as it appears in the file LMPBE221.MOD

```
NO2 + HV = NO + O
O + O2 + M = O3 + M
O + NO2 = NO + O2
O + NO2 = NO3 + M
O3 + NO = NO2 + O2
O3 + NO2 = O2 + NO3
NO + NO3 = #2 NO2
NO + NO + O2 = #2 NO2
NO2 + NO3 = N2O5
N2O5 + #RCON8 = NO2 + NO3
N2O5 + H2O = #2 HNO3              ! 298K only
NO2 + NO3 = NO + NO2 + O2
NO3 + HV = NO + O2
NO3 + HV = NO2 + O
O3 + HV = O + O2
O3 + HV = O*1D2 + O2
O*1D2 + H2O = #2 HO.
O*1D2 + M = O + M
HO. + NO = HONO
HONO + HV = HO. + NO
HO. + NO2 = HNO3
HO. + HNO3 = H2O + NO3        ! 1 ATM ONLY.
HO. + CO = HO2. + CO2         !1 ATM ONLY
HO. + O3 = HO2. + O2
HO2. + NO = HO. + NO2
HO2. + NO2 = HNO4
HNO4 + #RCON24 = HO2. + NO2
HNO4 + HO. = H2O + NO2 + O2
HO2. + O3 = HO. + #2 O2
HO2. + HO2. = HO2H + O2
HO2. + HO2. + M = HO2H + O2
HO2. + HO2. + H2O = HO2H + O2 + H2O
HO2. + HO2. + H2O = HO2H + O2 + H2O       !(1 ATM ONLY)
NO3 + HO2. = HNO3 + O2
NO3 + HO2. + M = HNO3 + O2
NO3 + HO2. + H2O = HNO3 + O2 + H2O
NO3 + HO2. + H2O = HNO3 + O2 + H2O        !(1 ATM ONLY)
HO. + HO2. = H2O + O2
RO2. + NO = NO
RO2. + HO2. = HO2. + RO2-HO2-PROD
```

Table 6-2 (Continued)

Listing of the chemical reactions involved in the LMPBE221 chemical mechanism as it appears in the file LMPBE221.MOD

```
RO2. + RO2. = RO2-RO2-PROD
RCO3. + NO = CO2 + NO2 + HCHO + RO2-R. + RO2.
RCO3. + NO2 = PAN
RCO3. + HO2. = -OOH + CO2 + HCHO
RCO3. + RO2. = RO2. + #.5 HO2. + CO2 + HCHO
RCO3. + RCO3. = #2 "HO2. + CO2 + HCHO"
PAN = RCO3. + NO2
RO2-R. + NO = NO2 + HO2.
RO2-R. + HO2. = -OOH
RO2-R. + RO2. = RO2. + #.5 HO2.
RO2-R. + RCO3. = RCO3. + #.5 HO2.
RO2-N. + NO = RNO3
RO2-N. + HO2. = -OOH + MEK + #1.5 -C
RO2-N. + RO2. = RO2. + #.5 HO2. + MEK + #1.5 -C
RO2-N. + RCO3. = RCO3. + #.5 HO2. + MEK + #1.5 -C
R2O2. + NO = NO2
R2O2. + HO2. =
R2O2. + RO2. = RO2.
R2O2. + RCO3. = RCO3.
RO2-XN. + NO = -N
RO2-XN. + HO2. = -OOH
RO2-XN. + RO2. = RO2. + #.5 HO2.
RO2-XN. + RCO3. = RCO3. + HO2.
HCHO + HV = #2 HO2. + CO
HCHO + HV = H2 + CO
HCHO + HO. = HO2. + CO + H2O
HCHO + HO2. = HOCOO.
HOCOO. = HO2. + HCHO
HOCOO. + NO = -C + NO2 + HO2.
HCHO + NO3 = HNO3 + HO2. + CO
CCHO + HO. = RCO3. + H2O
CCHO + HV = CO + HO2. + HCHO + RO2-R. + RO2.
CCHO + NO3 = HNO3 + RCO3.
MEK + HO. = H2O + #.5 "CCHO + HCHO" + RCO3. + &
#1.5 "R2O2. + RO2." + #.5 -C
MEK + HV + #QY.MEK = RCO3. + CCHO + RO2-R. + RO2.
RNO3 + HO. = NO2 + #.155 MEK + #2.055 CCHO + &
#.16 HCHO + #.11 -C + &
#1.39 "R2O2. + RO2."
MGLY + HV = HO2. + CO + RCO3.
MGLY + HV + #.107 = HO2. + CO + RCO3.
```

Table 6-2 (Continued)

Listing of the chemical reactions involved in the LMPBE221 chemical mechanism as it appears in the file LMPBE221.MOD

```
MGLY + HO. = CO + RCO3.
MGLY + NO3 = HNO3 + CO + RCO3.
HO. + CRES = #.15 RO2-XN. + #.85 RO2-R. + &
#.2 MGLY + #.085 CRES + RO2. + &
#5.805 -C
NO3 + CRES = HNO3 + -NO2 + #.5 CRES + #3.5 -C
HO. + AFG2 = RCO3.
AFG2 + HV = HO2. + CO + RCO3.
-NO2 + NO2 = -N
-NO2 + HO2. =
-NO2 =
HO. + AAR1 = #A1RR RO2-R. + #A1NR RO2-N. + &
#A1RXN RO2-XN. + #A1RH HO2. + &
#A1R2 R2O2. + #A1RO2 RO2. + #A1A1X HCHO + &
#A1A2X CCHO + #A1K4X MEK + #A1CO CO + &
#A1C2 CO2 + #A1CRES CRES + #A1MG MGLY + &
#A1U2 AFG2 + #A1XC -C
HO. + AAR2 = #A2RR RO2-R. + #A2NR RO2-N. + &
#A2RXN RO2-XN. + #A2RH HO2. + &
#A2R2 R2O2. + #A2RO2 RO2. + #A2A1X HCHO + &
#A2A2X CCHO + #A2K4X MEK + #A2CO CO + &
#A2C2 CO2 + #A2CRES CRES + #A2MG MGLY + &
#A2U2 AFG2 + #A2XC -C
HO. + AAR3 = #A3RR RO2-R. + #A3NR RO2-N. + &
#A3RXN RO2-XN. + #A3RH HO2. + &
#A3R2 R2O2. + #A3RO2 RO2. + #A3A1X HCHO + &
#A3A2X CCHO + #A3K4X MEK + #A3CO CO + &
#A3C2 CO2 + #A3CRES CRES + #A3MG MGLY + &
#A3U2 AFG2 + #A3XC -C
HO. + AAR4 = #A4RR RO2-R. + #A4NR RO2-N. + &
#A4RXN RO2-XN. + #A4RH HO2. + &
#A4R2 R2O2. + #A4RO2 RO2. + #A4A1X HCHO + &
#A4A2X CCHO + #A4K4X MEK + #A4CO CO + &
#A4C2 CO2 + #A4CRES CRES + #A4MG MGLY + &
#A4U2 AFG2 + #A4XC -C
ETHE + HO. = #.22 CCHO + #1.56 HCHO + RO2-R. + RO2.
ETHE + O3 = HCHO + #.37 O3OL-SB + #.44 CO + &
#.56 -C + #.12 HO2.
ETHE + O = HCHO + CO + HO2. + RO2-R. + RO2.
ETHE + NO3 = NO2 + #2 HCHO + R2O2. + RO2.
OLE1 + HO. = #O1P1R HCHO + #O1P23R CCHO + &
#O1P45R MEK + #O1PR RO2-R. + &
```

Table 6-2 (Continued)

Listing of the chemical reactions involved in the LMPBE221 chemical mechanism as it appears in the file LMPBE221.MOD

```
#01PN RO2-N. + RO2. + #010HXC -C
OLE1 + O3 = #0103A1 HCHO + #0103A2 CCHO + &
#0103K4 MEK + #0103MG MGLY + &
#0103CO CO + #0103SB O3OL-SB + &
#0103RH HO2. + #0103OH HO. + &
#0103RR RO2-R. + #0103R2 R2O2. + &
#0103RO2 RO2. + #0103PS RCO3. + &
#0103XC -C
OLE1 + O = #.4 HO2. + #.5 MEK + #.75 CCHO + #010AXC -C
OLE1 + NO3 = NO2 + #01P1 HCHO + #01P23 CCHO + &
#01P45 MEK + R2O2. + RO2. + #01N3XC -C
SO2 + HO. = HO2. + H2SO4
O3OL-SB + H2O =
O3OL-SB + SO2 = H2SO4
```

$$k_{A\nu} = \int_{\infty}^{0} \sigma\,[\lambda,T(h)]\;\phi[\lambda,T(h)]\;I[\lambda,N(T),\underline{X}]\;d\lambda \qquad (6\text{-}9)$$

where σ is the wavelength (λ) and temperature (T(h)) dependent absorption cross section coefficient, ϕ is the wavelength and temperature dependent quantum yield, and I is the actinic irradiance corresponding to the atmospheric state N at spatial location X.

The absorption coefficients and quantum yields are input as part of the chemical mechanism (i.e., LMPBE221.MOD). The photolysis constants at ground level are calculated in the subroutine NEWPHK by numerically integrating Eq (6-9). The photolysis rate constants as a function of height are calculated by empirical correlations using the surface values and the change in solar actinic flux with height, as shown in Carmichael et al. (1986). The solar intensity is based on the work of Peterson (1976) and calculated based on Julian date, time and latitude.

The water vapor concentration as a function of height is calculated according to the polynominal expression of Richardson (1971). This calculation is performed in subroutine WATCON.

6.4 Sample Results Using the Updated Chemical Integration Formulation

Several test calculations using the above procedures have been conducted in order to compare directly the results of the two different integration options. The first simulation consisted of the integration of the chemical mechanism listed in Table 6-2 in a box model with constant solar intensity with a solar zenith angle of zero and T=300 °K. The initial conditions are listed in Table 6-3 along with the results after 720 minutes using the two different integration methods., i.e., the hybrid solver and the QSSA method. The results of the predicted concentrations are very similar. However, the CPU time for the hybrid method is 27 seconds compared with 16 sec for the QSSA method. In terms of the mass balances, both methods conserve the sulfur and carbon mass very well, while the hybrid solver shows ~ 8% increase in the mass of nitrogen.

Table 6-3

Comparison of the Results Obtained using the Hybrid Solver and the QSSA Method for Constant Solar Angle Conditions

Concentrations (ppm) at t=720 min

	Hybrid	**QSSA**
O_3	3.78×10^{-1}	3.82×10^{-1}
NO	$1.3.8 \times 10^{-4}$	1.40×10^{-4}
NO_2	3.32×10^{-3}	3.4×10^{-3}
PAN	2.34×10^{-2}	2.41×10^{-6}
SO_2	8.26×10^{-2}	8.26×10^{-2}
Sulfate	1.73×10^{-2}	1.72×10^{-2}
H_2O_2	2.73×10^{-2}	2.39×10^{-2}
HNO_3	5.16×10^{-2}	5.12×10^{-2}
CPU Time	27 sec	16 sec

Mass Balance	t=0	t=720 min	t=720 min
S	0.100	0.100	0.100
C	3.239	3.27	3.235
N	0.0833	0.09068	0.08396

Initial Conditions (ppb) used in the Simulation from SOUBE221.EMO

Ethe 23.6	MGLY = 0	NO = 62.5
CO = 2321	AFG2 = 0	NO_2 = 20.8
HCHO = 8.3	AAR1 = 84.3	SO_2 = 100
CCHO = 3.6	AAR2 = 28.5	
MEK = 6.3	AAR3 = 13.0	
RNO_3 = 0	AAR4 = 7.2	
PAN = 0	AAR4 = 7.2	
CRES = 0	OLE1 = 20.4	

The second test calculation used slightly different initial conditions (as prepared from CALBE221 EMO emissions) and allowed the solar flux to vary diurnally starting at 6:00 a.m. The results using the hybrid solver and the QSSA method are compared in Table 6-4. The predictions using the hybrid and the QSSA method are similar with the maximum deviation of 10% between the calculated H_2O_2 levels. Once again the hybrid method shows a slight (~4%) increase in the mass of nitrogen.

Table 6-4

Comparison of Results Obtained using the Hybrid Solver and the QSSA Method for Conditions with a Diurnal Variation in Solar Flux

Concentrations (ppb) at t = 720 min

	Hybrid	**QSSA**
O_3	1.94×10^{-1}	1.92×10^{-1}
NO	2.99×10^{-3}	2.87×10^{-3}
NO_2	3.27×10^{-2}	3.10×10^{-2}
PAN	1.19×10^{-2}	1.13×10^{-2}
SO_2	9.46×12^{-2}	9.47×10^{-2}
Sulfate	5.42×10^{-3}	5.30×10^{-3}
H_2O_2	1.40×10^{-4}	1.21×10^{-4}
HNO_3	3.21×10^{-2}	3.14×10^{-2}

Mass Balance	**t=0**	**t=720min**	**t=720min**
S	0.100	0.100	0.100
C	3.08	3.09	3.08
N	0.0833	0.0866	0.0832

Initial Conditions (ppb)

ETHE = 23.6	MGLY = 0	NO = 62.5
CO = 2199	AIG2 = 0	NO_2 = 20.8
HCHO = 6.8	AAR1 = 84.3	SO_2 = 100
CCHO = 3.4	AAR2 = 28.5	
MEK = 6.3	AAR3 = 13.0	
RNO_3 = 0	AAR4 = 7.2	
PAN = 0	OLE 1 = 20.4	
CRES = 0		

References

Bjurel, G., G.G. Dahlquist, B. Lindberg, and S. Oden, (1970). Survey of Stiff Ordinary Differential Equations, Report No. NA70-11, Department of Information Processing, the Royal Inst. of Tech., Stockholm, Sweden.

Boris, J.P. and D.L. Book 1973. Flux-corrected transport. I. SHASTA, A fluid transport algorithm that works. J. Comp. Phys., 11 38-69.

Briggs, G., 1973. Internal memo as reported by F.A. Gifford Jr. in Turbulent Diffusion-Typing Schemes: A Review. Nucl. Saf., 17, 68-86, 1976.

Businger, J.A., 1973. Turbulent Transfer in the Atmospheric Surface Layer. Workshop on Micrometeorology, AMS, Boston, 1-28.

Businger, J.A., 1982. Equations and Concepts. Atmospheric Turbulence and Air Pollution Modeling (F.T.M. Nieuwstadt and H. van Dop, eds.), D. Reidel, Dordrecht, 1-36.

Carmichael, G.R., T. Kitada, and L.K. Peters, 1980. Application of a Galerkin finite element method to atmospheric transport problems. Computers and Fluids, 8: 155-176.

Carmichael, G.R., L.K. Peters, and T. Kitada, 1986. A Second Generation Model for Regional-Scale Transport/Chemistry/Deposition, Atmos. Environ., 20, 173-188.

Carter, W., 1988. Documentation for the SAPRC Atmospheric Photochemical Mechanism Preparation and Emissions Processing Programs for Implementation in Airshed Models, Draft report for California Air Resources Board.

Chock, D.P. and A.M. Dunker 1982. A Comparison of Numerical Methods for Solving the Advection Equation. General Motors Report No. GMR-3603/ENV#100 and Atmos. Environ., 17, 11-24.

Chock, D.P., 1985. A Comparison of numerical schemes for solving the advection equation II, Atmos. Environ., 19, 571.

Christensen O., and L.P. Prahm, 1976. A pseudo-spectral method for dispersion of atmospheric pollutants, J. Appl. Meteor., 15, 1284

Curtiss, C.F. and J.O. Hirschfelder, 1952. Integration of Stiff Equations, Proc. of National Acad. Sci., U.S.A., 38, 3, 235.

Dahlquist, G.G., 1963. A Special Stability Problem for Linear Multistep Methods, BIT 3, 27-43.

Egan B.A., and J.R. Mahoney, 1972. Numerical modeling of advection and diffusion of urban area source pollutants, J. Appl. Meteor., 11, 312-322.

Enright, W.H., T.E. Hull, and B. Lindberg, 1975. Comparing Numerical Methods for Stiff Systems of ODE's, Bit 15, 10-48.

Forester, C.K., 1977. Higher order monotonic cconvection difference schemes. J. Comp. Phys. 23: 1-22

Fowler, D. and M.H. Unsworth, 1979. Turbulent transfer of sulphur dioxide to a wheat crop. Q. J. Roy. Meteor. Soc., 105, 767-784.

Gear, C.W., 1971. Numerical Initial Value Problems in Ordinary Differential Equations. Englewood Cliffs, N.J.: Prentice Hall.

Gelinas, R.J., 1972. Stiff Systems of Kinetic Equations, J. of Comput. Physics, 9, 222-236.

Haan B. de, 1981. A comparison of finite difference schemes, describing the two-dimensional advection equation, in: Air Pollution Modeling and its Application I, C. de Wispelaere, ed., Plenum Press, New York.

Hanna, S.R., 1982. Applications in Air Pollution Modeling. Atmos. Turbulence and Air Poll. (eds. F.T.M. Nieuwstadt and H. Van Dop), D. Reidel, Dordrecht, 275-310.

Hanna, S.R., J.C. Weil and R.J. Paine, 1986. Plume Model Development and Evaluation. Hybrid Approach Final Report. EPRI, Palo Alto, CA.

Hesstvedt, E., O. Hov, and I.S.A. Isaksen, 1978. Quasi-steady-state approximations in air pollution modeling, Comp. J. Chem. Kinetics, Vol. X, 971-994.

Hicks, B.B., 1982. In: Critical Assessment Document on Acid Deposition (Chapter VII-Dry Deposition). ATDL Contribution File No. 81/24. Atmospheric Turbulence and Diffusion Laboratory, NOAA, Oak Ridge, TN.

Holtslag, A.A.M. and F.T.M. Nieuwstadt, 1986. Scaling the Atmospheric Boundary Layer. Bound. Lay. Meteorol., 36, 201-209.

Holtzworth, G.C., 1972. Mixing Heights, Wind Speeds, and Potential for Urban Air Pollution Throughout the Contiguous United States. Pub. No. AP-101, U.S. EPA, Research Triangle Park, NC.

Hosker, R.P., 1974. A Comparison of Estimation Procedures for Overwater Plume Dispersion. Proceedings of the Symposium on Atmospheric Diffusion and Air Pollution. American Meteorological Society, Boston, MA.

Hosker, R.P., Jr. and S.E. Lindberg, 1982. Review: Atmospheric Deposition and Plant Assimilation of gases and Particles. Atmospheric Environ., 16, 889-910.

Lamb, R.G., W.R. Shu, D.R. Duran, J.H. Seinfeld, L.E. Reid, 1980. Continental Research in Mesoscale Air Pollution Simulation Modeling - Vol. VI: Further Studies in the Modeling of Microscale Phenomena. SAI Report EF77-143R.

Lamb, R.G., 1984. A regional scale (1000 km) model of photochemical air pollution. Part 1 Theoretical formulation. EPA draft report.

Lapidus, L. and Schiesser, W.E., Ed., 1976. Numerical Methods for Differential Systems, Academic Press, Inc. New York.

Long, P.E. and D.W. Pepper 1976. A comparison of six numerical schemes for calculating the advection of atmospheric pollution. Third Symposium on Atmospheric Turbulence, Diffusion, and Air Quality, Raleigh, NC. Oct. 19-22.

Long, P.E. and D.W. Pepper 1981. An examination of some simple numerical schemes for calculating scalar advection. J. Appl. Meteor., 20, 146-156.

Lurmann, F.W., A.C. Lloyd, and R. Atkinson, 1986. A Chemical Mechanism for use in Long-Range Transport/Acid Deposition Computer Modeling, JGR, 91, 10905.

Mahrer, Y. and R.A. Pielke 1978. A test of an upstream spline interpolation technique for the advection terms in a numerical mesoscale model. Mon. Wea. Rev., 106, 818-830.

Marchuk, G.I. 1975. Methods of Numerical Mathematics. New York: Springer-Verlag. 316 pp.

McRae, G.J., 1981. Mathematical Modeling of Photochemical Air Pollution. Ph.D. Thesis, California Institute of Technology, Pasadena, CA.

McRae, G., W. Goodin, and J. Seinfeld, 1982. Numerical Solution of the Atmospheric Diffusion Equation for Chemically Reacting Flows, J. Comp. Phys., 95, 1-42.

Moller, U. and G. Shumann, 1970. Mechanisms of transport from the atmosphere to the earth's surface. J. Geophy. Res., 75, 3013-3019.

Nieuwstadt, F.T.M., 1984. The turbulent structure of the stable, nocturnal boundary layer. J. Atm. Sci., 41, 2202-2216.

O'Dell, R.A., M. Taheri, and R.L. Kabel, 1977. A model for uptake of pollutants by vegetation. JAPCA, 27, 1104-1109.

Pepper, D.W., C.D. Kern, and P.E. Long 1979. Modeling the dispersion of atmospheric pollution using cubic splines and chapeau functions. Atmos. Environ. 13, 223-237.

Peterson, J.T., 1976. Calculated Actinic Fluxes (290-700 nm) for Air Pollution Photochemistry Applications, EPA-60014-76-025.

Pleim, J., A. Venkatram and R.J. Yamartino, 1984. The Dry Deposition Model. Volume 4. ADOM/TADAP Model Development Program. Ontario Ministry of the Environment, Rexdale, Ontario, Canada.

Reynolds, S.D., T.W. Tesche, and L.E. Reid, 1979. An Introduction to the SAI

Airshed Model and its Usage. SAI Report EF78-53R4 - EF79-31.

Richards, J.M., 1971. A Simple Expression for the Saturation Vapor Pressure of Water in the Range - 50 to 140 C, British J. Applied Physics D, 4, L25 - L18.

Roache, P.J., 1976. Computational Fluid Dynamics (2nd Edition). Albuquerque, NM: Hermosa Publishers. 434 pp.

Schere, K.L., 1983. An evaluation of several numerical advection schemes. Atmos. Environ., 17, 1897-1907.

Scire, J.S. and F.W. Lurmann, 1983. Development of the MESOPUFF-II Dispersion Model. Proc. AMS Sixth Symposium on Turbulence and Diffusion, March 22-25, Boston, MA.

Scire, J.S., F.W. Lurmann, A. Bass, and S. Hanna, 1984. Development of the MESOPUFF II Dispersion Model. EPA-600/3-84-057. U.S. Environmental Protection Agency, Research Triangle Park, NC, 82 pp.

Scire, J.S. and R.J. Yamartino, 1984. Design and Structure of the ADOM/TADAP Driver Program. Volume 2, ADOM/TADAP Model Development Program, Ontario Ministry of the Environment, Rexdale, Ontario, Canada.

Sehmel, G.A. and S.L. Sutter, 1974. Particle deposition rates on a water surface as a function of particle diameter and air velocity. J. Rechs Atmos. III, 911-918.

Sehmel, G.A., 1980. Particle and Gas Dry Deposition - A Review. Atmos. Environ., 14, 983-1011.

Seinfeld, J.H., I. Lepidus, and M. Hwang, 1970. Review of Numerical Integration Techniques for Stiff Ordinary Differential Equations, Ind. Eng. Chem. Fundam., 9, 2, 266.

Shepherd, J.G., 1974. Measurements of the direct deposition of sulphur dioxide onto grass and water by the profile method. Atmos. Environ., 8, 69-74.

Shieh, D. 5-5, 1983. The Evaluation of Numerical Techniques for Solution of Stiff Ordinary Differential Equations Arriving from Chemical Kinetics Problems. M.S. Thesis, Chemical and Materials Engineering Program, University of Iowa.

Shieh, D., Y. Chang, and G.R. Carmichael, 1988. The Evaluation of Numerical Techniques for Solution of Stiff Ordinary Differential Equations Arising from Chemical Kinetics Problems, Env. Software, in Press.

Slinn, S.A. and W.G.N. Slinn, 1980. Predictions for particle deposition on natural waters. Atmos. Environ., 14, 1013-1016.

Slinn, W.G.N., L. Hasse, B.B. Hicks, A.W. Hogan, D. Lal, P.S. Liss, K.O. Munnich, G.A. Sehmel, and O. Vittori, 1978. Some aspects of the transfer of atmospheric trace constituents past the air-sea interface. Atmos. Environ., 12, 2055-2087.

Smagorinsky, J., 1963. General circulation experiments with the primitive equations: 1. The basic experiment. Mon. Wea. Rev. 91: 99-164.

Smolarkiewicz, P.K., 1984. A fully multidimensional positive definite advection transport algorithm with small implicit diffusion, J. Comp. Phys., 54, 325.

Stull, R.B., 1984. Transilient turbulence theory. Part 1: The concept of eddy mixing across finite distances. J. Atmos. Sci., 41, 3351-3367.

Tennekes, H., 1982. Similarity Relations, Scaling Laws, and Spectral Dynamics. Atmospheric Turbulence and Air Pollution Modeling (F.T.M. Nieuwstadt and H. van Dop, eds.), D. Reidel, Dordrecht, 37-68.

U.S. EPA, 1987. Industrial Source Complex (ISC) Dispersion Model User's Guide - Second Edition (Revised). EPA-450/4-88-002.

van Eykeren, J., Th. van Stijn and N. Praagman, 1987. A comparative investigation of numerical methods for advective processes. Air Pollution Modeling and Its Application VI, H. van Dop (Ed.) Plenum Press, New York, 641-652.

Voldner, E.C., L.A. Barrie, and A. Sirois, 1986. A literature review of dry deposition of oxides of sulphur and nitrogen with emphasis on long-range transport modeling in North America. Atmos. Environ., 20, 2101-2123.

Warner, D.D., 1977. The Numerical Solution of the Equations of Chemical Kinetics, J. Phys. Chem., 81, 25, 2329.

Wesely, M.L. and B.B. Hicks, 1977. Some factors that affect the deposition rates of sulfur dioxide and Similar gases on Vegetation. J. Air Poll. Control Assoc., 27, 1110-1116.

Willoughby, R.A., Ed., 1974. Stiff Differential Systems, The IBM Research Symposia Series, Plenum Press, New York, NY.

Wyngaard, J.C., 1985. Structure of the Planetary Boundary Layer and Implications for its Modeling. J. Clim. and Appl. Meteorol., 24, 1111-1130.

Wyngaard, J.C., 1988. Structure of the PBL. Lectures on Air Pollution Modeling, AMS, Boston, 9-62.

Yamartino, R.J. and J.S. Scire, 1984. The Transport and Diffusion Modules, Volume 3, ADOM/TADAP Model Development Program, Ontario Ministry of the Environment, Rexdale, Ontario, Canada.

Yamartino, R.J., 1985. Atmospheric Pollutant Deposition Modeling. Chapter 27 in Handbook of Applied Meteorology, David D. Houghton, Editor. John Wiley and Sons, New York, 1461 pp.

Yanenko, N.N., 1971. The Method of Fractional Steps, Springer, New York.

Young, T.R. and J.P. Boris, 1977. A Numerical Technique for Solving Stiff Ordinary Differential Equations Associated with the Chemical Kinetics of Reaction Flow Problems, J. Phys. Chem., 82, 2424.

Zalesak, S.T., 1979. Fully multidimensional flux-corrected transport algorithms for fluids. J. Comp. Phys., 31, 335-362.

CARB LIBRARY
05221